Journal of Volcanology and Geothermal Research
August 2013, Volume 264, Pages 72–84
http://dx.doi.org/10.1016/j.jvolgeores.2013.07.005

Temporal source evolution and crustal contamination at Lopevi Volcano, Vanuatu Island Arc

Aurélien Beaumais[a], Gilles Chazot[a, *], Laure Dosso[b], Hervé Bertrand[c]

[a] Université de Brest (UBO), UMR 6538, Domaines Océaniques, Institut Universitaire Européen de la Mer, place Copernic, 29280 Plouzané, France
[b] CNRS-UMR6538, Ifremer, Département Géosciences Marines, 29280 Plouzané, France
[c] UMR-CNRS 5570, Laboratoire de Géologie de Lyon, Ecole Normale Supérieure de Lyon et Université Lyon 1, 69364 Lyon, France

*: Corresponding author : Gilles Chazot, email address : Chazot@univ-brest.fr

Abstract:

Here we present a new geochemical study of Lopevi volcano, one the most active volcanoes in the Vanuatu island arc. We focus on the temporally well-defined sequence of lava flows emitted since 1960, and for the first time, on pre-1960 volcanic products, including high-MgO basalts and felsic andesites, the most evolved lavas sampled so far on this island. This work reports the first Pb and Hf isotopic study of lavas from Lopevi island. These lavas display correlations between differentiation indexes such as SiO_2 content and isotopic ratios. The felsic andesites extend the known correlations with both the least (Sr–Pb) and the most (Nd–Hf) radiogenic isotopic compositions on the island. Our results confirm that the rising magma interacted with the sub-arc crust. Assimilation–Fractional Crystallization (AFC) quantitative modeling of trace element ratios and isotopic compositions requires 1% and 10% of assimilated partial melts of a mafic oceanic crust to account for the pre- and post-1960 lavas, respectively. The post-1960 lavas differ from the former lavas emitted ~ 20 years earlier by enrichments in fluid mobile elements (K, Ba, Rb…), Th, and Light Rare Earth Elements (LREE). We ascribe these features to slight variations in the metasomatic agent added to the sub-arc mantle and ultimately derived from the subducted lithosphere. However, the contrasting time scales involved in subducted lithosphere dehydration and magma genesis, relative to the time elapsed between eruptions of the two lava series, suggest that two different portions of mantle which have undergone slightly different metasomatism, gave birth to the Lopevi lavas. These distinct magmas are still present beneath the volcano.

Highlights

► New geochemical study with Hf–Pb isotopes of Lopevi, including recent and old lavas ► Evidences for interactions between ascending magmas and sub-arc crust ► Evidence for short time scale mantle source variations (~ 20 years) ► Involvement of a different metasomatic agent in the pre- and post-1960 lavas

Keywords: Lopevi ; Vanuatu ; Geochemistry ; Isotopes ; Subduction ; Mantle source

1. Introduction

Intra-oceanic arcs are a privileged target for understanding the subduction process and for investigating the mantle source(s) of associated magmatism, because in this context the crustal contamination of mantle derived magmas is limited compared to the active continental margins setting, where the crust is thicker and chemically heterogeneous (e. g., Hildreth and Moorbath, 1988 and Woodhead, 1989). However the magnitude of this contamination process remains poorly constrained in these intra-oceanic arcs and is not easy to identify due to potentially similar chemical and isotopic compositions between the contaminant (the oceanic crust) and the rising magmas.

The Vanuatu island arc is an intra-oceanic arc where near-primitive magmas such as picrites, ankaramites or high MgO basalts are commonly erupted at several volcanic centers, giving the opportunity to observe a straightforward geochemical mantle source signature.

According to along-arc geochemical studies, the Vanuatu lava compositions vary from low K tholeiite to shoshonite series, with some high Mg andesites emitted in the southernmost seamounts (Monzier et al., 1997). Isotopic studies suggest that Indian and Pacific mantle reservoirs coexist beneath the Vanuatu island arc (Crawford et al., 1995). The high inter- and intra-islands geochemical variability observed is mainly related to elemental and isotopic heterogeneities in the sub-arc mantle wedge (Greene et al., 1994) and to variable addition of the subduction component along the arc (Peate et al., 1997). A few detailed studies have been focused on the origin of the primitive magmas and/or the geochemical evolution of a single volcanic system, on the scale of one island. Such studies include Merelava (Barsdell, 1988), Epi (Barsdell and Berry, 1990), Aoba (Eggins, 1993; Sorbadere et al., 2011), Efate (Raos and Crawford, 2004), Tanna (Métrich et al., 2011) and Lopevi (Handley et al., 2008).

We present a new geochemical study of the Lopevi volcano (Figure 1), based on the temporally well-defined sequence of lava flows emitted since 1960, and on older lavas which include high MgO basalts as well as andesites, the most evolved rocks found on the island. This study reports for the first time geochemical data on pre-1960 samples and the first Pb and Hf isotopic compositions from Lopevi Island.

2. Geological setting and previous work

The Vanuatu arc is made up of three parallel chains of volcanic islands located along the boundary of the SW Pacific plate: the western belt, the eastern belt, and the presently active central chain (Fig. 1). The aerial part of the Vanuatu central arc stretches along 1200 km from Ureparapara in the north to Hunter in the south. It is the surface expression of the fast subduction of the Australia plate beneath the North Fiji Basin which reaches 118 $mm.a^{-1}$ at Tanna (Taylor et al., 1995; Calmant et al., 2003).

Tectonics of the SW Pacific is marked by the confrontation between the two large Australia and Pacific plates. The present convergence is characterized by a large deformed area of more than 1000 km, the North Fiji Basin and is expressed by two opposite subductions: the westward Tonga-Kermadec and the eastward Solomon-Vanuatu. This is the result of a 25 m.y. long and complex tectonic history (MacFarlane et al., 1988; Greene et al., 1994). Ancient westward subduction of the Pacific plate beneath the Australia plate has given birth to the Vitiaz volcanic arc (25-14 Ma) from the Solomon to the Tonga islands and corresponds to the Western Belt (Mitchell and Warden, 1971) as shown in figure 1a, b. This subduction probably stopped when the Ontong-Java plateau collided with the Solomon Islands in the north (Meffre and Crawford, 2001; Mann and Taira, 2004).

As convergence continued, the North Fiji Basin began to open ~12 Ma ago (Auzende et al., 1995). This convergence is marked 7 million years ago by the eastward diving of the Australia plate beneath the North Fiji Basin at the present place of the Vanuatu trench, giving birth to the Eastern Belt (Fig. 1a). At ~ 6 Ma, the active volcanic arc (Central Chain) moved closer to the trench, in response to the steepening of the slab diving angle to 70° (Pascal et al., 1978).

Between 3 and 1.5 Ma, the subduction-collision of the D'Entrecasteaux Ridge (an ancient Eocene arc) near Epi latitude (South of Lopevi) was a major tectonic event, producing a transverse fault system by compression in the central part of the arc (Collot et al., 1985; Greene et al., 1994). The collision zone shifted northward and is now located in front of Aoba (Fig. 1b), marked by the lack of trench and by the deceleration of the subducting plate to 3.5 cm.a^{-1}. A slab detachment between Ureparapara and Vanua Lava in the north and between Ambrym and Efate occurred within the last million years (Châtelain et al., 1992; Monzier et al., 1997). Further south, the Loyalty ridge still collides with the Vanuatu arc close to 22°S (Monzier et al., 1993). The North Loyalty basin, composed of a Middle Eocene oceanic crust overlain by ~ 650 m of mainly volcanoclastics sediments (Andrew et al., 1973), is currently subducting at 9 cm.a^{-1} in front of Efate.

Strong geochemical variations along the Vanuatu arc have been well described by several groups based on major and trace element contents (Barsdell et al., 1982; Dupuy et al., 1982; Monzier et al., 1997; Peate et al., 1997) and Sr, Nd, Pb, and Hf isotopic compositions (Briqueu et al., 1994; Crawford et al., 1995; Peate et al., 1997; Laporte et al., 1998; Turner et al., 1999; Pearce et al., 2007; Heyworth et al., 2011). Low K arc-tholeiites erupted before 2-3 Ma, are described as “normal suites” and show a Pacific-like mantle isotopic signature. Since the onset of the subduction-collision of the D’Entrecasteaux Ridge, lavas are characterized by a strong enrichment in K_2O, large ion lithophile elements (LILE), and LREE and by an isotopic composition shifted toward an Indian-like mantle signature with radiogenic Sr and high $^{207}Pb/^{204}Pb$ and $^{208}Pb/^{204}Pb$ isotope ratios (Dupuy et al., 1982; Briqueu et al., 1994; Baker and Condliffe, 1996; Monzier et al., 1997; Peate et al., 1997; Laporte et al., 1998). The most recent studies argue for a westward upwelling of an enriched asthenospheric mantle from the back arc in front of the D’Entrecasteaux collision zone to explain the observed chemical differences (Monzier et al., 1997; Peate et al., 1997; Pearce et al., 2007; Heyworth et al., 2011).

Lopevi is one of the most active volcanoes of the archipelago. This small conical island, 7 km large and rising up to 1413 m, is composed of two distinct cones. The older one presents a summit crater with little fumarole activity. The most recent crater, 1150 m high, appeared during the 1963 eruptive phase (Williams and Curtis, 1964; Warden, 1967) and is breached to the NW. This strato-volcano has been active since historical time both at summit and flank vents, with different eruption styles, including explosive basaltic sub-plinian eruptions associated with pyroclastic flows (e.g. 1960 and 2003 eruptions) and effusive activities. The later produced lava flows that reached the coast and came mainly from the 1963 parasitic crater or from excentric vents opened on the western flank along a NW-SE-trending fissure system (Warden, 1967). Eruptive cycles of 15 to 20 years have been observed since the mid-

19th century. The last major eruptions occured in 1939, 1960-1965, 1980, and 1998-2008. Lopevi shows a strong tectonic control, as the neighbouring island of Ambrym (Picard et al., 1995) since these volcanoes are constructed on transverse fractures (Greene et al., 1988) which are interpreted as major active transcurrent wrench faults related to the D'Entrecasteaux Ridge collision (Fig.1).

3. Sampling and analytical techniques

Thirty five samples from different lava flows were collected on the Lopevi island during fieldwork in September 2008 and 2009 (Fig. 2). Samples are more or less vesicular basalts and basaltic andesites with a porphyritic texture. Some samples belong to the well defined post-1960 activity while others pre-1960 samples were collected around the older summit crater and in deep gullies in the older part of the island. Some more differentiated samples such as andesitic pebbles are found along beaches south of the island, at the lower part of gullies. All samples are very fresh, with loss on ignition values (LOI) lower than 0.5 wt %.

3.1. Major and trace elements

All samples were analysed for major and trace elements. Major element analyses of whole rock samples were performed on glass fusion beads by X-Ray Fluorescence spectrometry using a Philips PW 1404 (LGL, Lyon). Relative standard deviations are 1% for SiO_2 and 2% for the other major elements, except for low concentrations (< 0.50%) for which the absolute standard deviation is 0.01. Major element compositions for minerals (phenocrysts and microlites) of 12 samples were carried out on thin sections with a Cameca SX100 Electron

Probe Micro Analysis (Centre Microsonde Ouest - Plouzané). The operating conditions were 15 kV accelerating voltage, 10 nA beam current, and 15-30 s counting time according to the element.

Trace element concentrations were determined in solution by HR-ICP-MS Thermo Fisher Element-II® (IUEM, Plouzané). Samples were measured according to the procedures described by Barrat et al. (1996) and by Chauvel et al. (2011). Trace element concentrations were calculated using a machine drift correction based on the 1-element (Tm) or 3-element (Be, In, Tm) spike with a mass-based interpolation. Precision for most elements is better than 2 % RSD (3 % RSD for U and Th). Accuracy is better than 5 % for most elements relative to suggested values for international standards BCR-2 (Jochum and Brueckner, 2008) and JB-2 (Peate et al., 2009) (Table 1).

3.2. Isotopes

Based on major and trace element concentrations, 15 samples were selected for Pb, Sr, Nd and Hf isotopic measurements. They are representative of the different volcanic phases of Lopevi and of the whole extent of magma differentiation. Chemical separation for isotopic measurements was carried out in a class 10000 clean room (Ifremer). From a single sample digestion, we used a combined procedure for separating Pb, Sr, Nd, and Hf in 5 steps chromatography. (1) About 700 mg of whole rock powder were dissolved for 72 h with a 3:1 concentrated HF-HBr mixture in teflon Savillex® beakers at about 80°C and evaporated to dryness. (2) Pb was first separated from other elements using the classical HBr-anion-exchange resin technique (AG1-X8 100-200mesh) of Manhes et al. (1984). (3) The Pb-free fraction obtained was loaded onto a ~6.5 cm^3 cation-exchange resin BioRad® (AG50-8X 200-400 mesh) to separate from the major elements the High Field Strength Elements (HFSE) with a mixed 0.5M HCl /0.15M HF, Sr with 3M HCl, and rare earth elements (REE) with 3.6M HNO_3. (4) Hf was further separated from Ti using a modified version of the method described by Yang et al. (2010). The HFSE fraction was loaded onto a column filled with 100 mg of Eichrom® Ln-resin. Ti was removed with 15 mL of 6M HCl-H_2O_2 mixture and the Hf-Zr fraction was eluted with 2 mL of 2M HF. (5) Finally Nd was isolated from the other REE using the Eichrom® Ln-resin technique adapted from Richard et al. (1976) with diluted HCl. Total procedural chemistry blanks during the course of this work were less than 58 pg for Hf, 5 pg for Nd, 143 pg for Sr, and 50 pg for Pb. These values are totally negligible relative to the amounts of element present in the samples.

Sr and Nd isotope ratios were measured in static mode using a solid source Thermo Fisher® Triton TI-MS (Thermo Ionization – Mass Spectrometer) at IUEM (Plouzané, France) and a MAT26X TI-MS (MAT261 upgraded by Spectromat) at Ifremer (Plouzané, France). All measured ratios were fractionation corrected using $^{88}Sr/^{86}Sr$ = 8.3752 and $^{146}Nd/^{144}Nd$ = 0.7219. The average $^{87}Sr/^{86}Sr$ ratio measured for the NBS 987 standard was 0.710271±14 (2SD, for 12 runs) on the Triton, and 0.710244±18 (2SD, for 5 runs) on the MAT26X. No correction was applied. The average $^{143}Nd/^{144}Nd$ ratio measured for the JNdi-1 standard was 0.512105±12 (2SD, for 13 runs) and 0.511846±7 (2SD, for 6 runs) for the La Jolla standard.

Pb and Hf isotopic ratios were measured using a Thermo Fisher® Neptune MC-ICP-MS (Multi Collector - Inductively Coupled Plasma – Mass Spectrometer) at IUEM. The Hf mass bias was corrected using an exponential law and assuming a $^{179}Hf/^{177}Hf$=0.7325. The average $^{176}Hf/^{177}Hf$ ratio measured for the JMC475 was 0.282152±11 (2SD, for 58 runs). Pb isotopic ratios were measured using the thallium addition technique in order to correct the mass bias (White et al., 2000). The NIST981 standard was run every two or three samples to correct all Pb isotopic ratios by standard bracketing with the value recommended by Galer and

Abouchami (1998). The average $^{206}Pb/^{204}Pb$, $^{207}Pb/^{204}Pb$, $^{208}Pb/^{204}Pb$ ratios measured for the NIST981 were respectively 16.930±3, 15.483±4, and 36.670±12 (2SD, for 29 runs).

4. Results

4.1. *Major and trace element results*

Lopevi lavas display a medium-K calc-alkaline series (Fig. 3) and are mostly basalts and basaltic andesites ranging from 49.5 to 56 wt % SiO_2, except for two acid andesite pebbles at ~61 wt % SiO_2 (only one data point visible in Fig. 3 because of their very similar chemical composition). Post-1960 lavas are slightly more enriched in K_2O than the older ones (Fig. 3). Basalts and basaltic andesites are composed of abundant euhedral to subeuhedral phenocrysts of clinopyroxene (Wo_{35-45}, Fs_{6-17}, En_{41-48}), plagioclase (An_{78-92}) and olivine (Fo_{70-90}), surrounded by a glassy to fine grained matrix composed of microcrysts of clinopyroxene (Wo_{7-37}, Fs_{14-36}, En_{26-66}), plagioclase (An_{30-89}), olivine (Fo_{60-78}) and Fe-Ti oxides. Phenocrysts from the basaltic-andesite LO14 show more evolved compositions with clinopyroxene (Wo_{8-37}, Fs_{33-66}, En_{42-61}), plagioclase (An_{55-85}) and olivine (Fo_{74}). Common tendency to aggregation of phenocrysts is observed. Andesites are composed of abundant tabular, sometimes zoned, plagioclases (An_{56-68}) and less abundant clinopyroxene phenocrysts (Wo_{36-39}, Fs_{15-20}, En_{40-46}). Olivine is absent and some scarce orthopyroxene phenocrysts (Wo_{2-3}, Fs_{31-52}, En_{44-65}) are found. Those phenocrysts are set in a fine grained matrix composed of microcrysts of plagioclase (An_{23-60}), clinopyroxene (Wo_{8-47}, Fs_{25-44}, En_{29-52}) and Fe-Ti oxide. Overall, crystals set in the more evolved rocks are impoverished in Mg and in Ca, compared to others, as observed also in the microcrysts compared to the phenocrysts in one sample.

Major element variation diagrams (Fig. 4) show that some basalts have relatively high MgO content reaching 7.8 wt % and that the post-1960 lavas are also slightly more enriched in Al_2O_3 than the older ones. MgO, Fe_2O_3, and CaO are negatively correlated with silica content, with a slope change at ~ 51 wt % SiO_2 for the post-1960 lavas and at ~ 52 wt % SiO_2 for the older ones, whereas Na_2O and K_2O show positive correlations (Figs. 3 and 4, Fe_2O_3, CaO, and Na_2O are not shown). Al_2O_3 is positively correlated with silica content for low SiO_2 values (< 51 - 52 wt %) and negatively correlated for higher values.

Chondrite-normalised rare earth element (REE) patterns (Fig. 5a) have slight to moderate enrichment in the Light REE (LREE ~ 20 to 30 times the chondritic values) relative to Heavy REE (HREE) which draw an almost flat pattern (~ 10 to 20 times the chondritic values). Pre- and post-1960 lavas show overall similar patterns, but the former display a larger range of compositions, in line with their higher Si content.

The extended trace element patterns (Fig. 5b) are typical of arc magmas with an enrichment in fluid mobile elements (Rb, Ba, U, K, Pb, Sr), and a depletion in high field strength elements (HFSE: Nb, Ta, Hf, Zr, Ti) relative to the REE. Overall post-1960 lavas are more homogeneous than the pre-1960 lavas. The high MgO basalt LO20 has the lowest trace element abundance, and its trace element pattern is slightly different from the others. Some lavas display negative Eu anomalies which are more developed in the most evolved lavas.

Lopevi lavas display a moderate enrichment in fluid mobile elements, and relatively low La/Yb ratio (2-3) compared to other Vanuatu island lavas such as those facing the D'Entrecasteaux ridge collision which display La/Yb ratios reaching ~ 12 (Fig. 5). Highly incompatible elements (such as Nb and Th) content increases during magmatic differentiation (Fig. 6). Pre- and post-1960 lavas display two distinct positive trends with distinct Th/Nb ratios (~ 0.45 vs. 0.55, respectively), supporting the existence of two slightly distinct magmatic series at Lopevi. However the felsic andesites, belonging to the pre-1960 group, are aligned on the post-1960 trend.

4.2. *Isotopic results*

The Lopevi samples show a restricted isotopic range compared to the whole range reported from Vanuatu volcanic islands (Fig. 7). Their $^{87}Sr/^{86}Sr$ ratios vary from 0.70392 to 0.70409. $^{143}Nd/^{144}Nd$ and $^{176}Hf/^{177}Hf$ ratios show very small variations from 0.51296 to 0.51303 and from 0.28316 to 0.28318, respectively. Variations in Pb isotopic compositions are also limited, and range from 18.44 to 18.51 for $^{206}Pb/^{204}Pb$, from 15.53 to 15.55 for $^{207}Pb/^{204}Pb$, and from 38.38 to 38.44 for $^{208}Pb/^{204}Pb$. This limited isotopic variation does not bring out significant isotopic differences between the pre- and the post-1960 lavas. However the new Sr-Nd isotopic analyses extend the compositional range reported by Handley et al. (2008) toward lower $^{87}Sr/^{86}Sr$ ratios and higher $^{143}Nd/^{144}Nd$ ratios recorded in the more differentiated products (Fig. 7a).

Lopevi lavas have relatively high $^{87}Sr/^{86}Sr$, $^{207}Pb/^{204}Pb$ and $^{208}Pb/^{204}Pb$ values, and intermediate $^{143}Nd/^{144}Nd$, $^{176}Hf/^{177}Hf$, and $^{206}Pb/^{204}Pb$ values compared to the isotopic composition range reported for the Vanuatu lavas (Peate et al., 1997; Laporte et al., 1998; Turner et al., 1999; Pearce et al., 2007). This isotopic signature is intermediate between the isotopic signatures of the lavas emitted in front of the collision zone and those emitted away in the northern and the southern part of the arc. Lopevi lavas fall broadly in the Indian MORB field in the Pb-Pb and Hf-Nd isotopic spaces, having high $^{207}Pb/^{204}Pb$ and $^{208}Pb/^{204}Pb$ values for a given $^{206}Pb/^{204}Pb$ value, and low $^{143}Nd/^{144}Nd$ ratio for a given $^{176}Hf/^{177}Hf$ value (Fig. 7). However, in the Sr-Nd space (Fig. 7a), Lopevi lavas plot outside the MORB fields, displaying higher $^{87}Sr/^{86}Sr$ ratios as commonly described in island arc lavas, and fall within the field of the North Loyalty Basin sediments.

5. Discussion

5.1. Fractional Crystallization

Lopevi arc lavas include only a small proportion of differentiated materials. Lopevi lavas host "classical" mineral assemblage: olivine, clinopyroxene, plagioclase, and Fe-Ti oxides. In the more evolved lavas, olivine disappears while orthopyroxene is present. No hydrous minerals like amphibole are present.

Major element covariation diagrams (Fig. 4) suggest by their trends and their inflections a two- stage crystallization. The first stage is characterized by the removal of olivine and clinopyroxene as seen by the decrease of MgO content from 8 to 5 % (Fig. 4). The inflection of the MgO-SiO_2 trend at 51-52 wt. % SiO_2 is related to the onset of Al_2O_3 decrease in the lavas and to plagioclase fractionation. This change is also recorded by the Eu negative anomaly (which is compatible in plagioclase) shown in the trace element patterns of the more evolved samples. Thereby the appearance of low-Ca orthopyroxene in the most evolved rocks is probably related to the abundance of plagioclase which integrates a large amount of CaO and the lack of elevated water pressure to stabilize amphibole.

Least square modelling of the major element data (Bryan et al., 1969) accounts successfully for the first stage of fractional crystallization in the most mafic rocks until 51 % SiO_2 and gives similar results to those of Handley et al. (2008), with a ~30 % degree of crystal fractionation. However the modelling fails to account for the second stage of crystallization, suggesting that an additional process is involved during magmatic differentiation. This is also suggested also by the change of Nb/Th ratios during the differentiation of the pre-1960 lavas (Fig. 6).

5.2. Assimilation – Fractional Crystallization (AFC)

5.2.1. Isotopic evidence

Classical long-lived radiogenic systems (Sr-Nd-Pb-Hf) are a powerful tool to spot magma contamination, provided that the isotopic composition of the contaminant is distinct from the composition of the magma. In spite of a rather restricted range in isotopic compositions, the Lopevi lavas display a negative Sr-Pb and a positive Nd-Hf correlation with the differentiation indexes (SiO_2, MgO, Th, La), extending the correlations reported in Handley et al. (2008) towards lower $^{87}Sr/^{86}Sr$, higher $^{143}Nd/^{144}Nd$ and higher SiO_2 values (Fig. 8, Hf isotopes not shown). It suggests that a contamination process occurred during the ascent of the magma toward the surface and that the contaminant is less (Sr and Pb) and more (Nd and Hf) radiogenic than the most evolved samples. This is in agreement with Handley et al. (2008) who identified contamination in the post-1960 lavas using Sr, Nd, Ra, and Th isotopes. These authors argued for the assimilation of a small degree of partial melt (2 – 10 %) of a >380 Ka old mafic oceanic crust, of MORB composition, rejecting the hypothesis of bulk assimilation of oceanic crust and magma mixing process.

5.2.2. AFC model

Contamination by the oceanic crust is investigated using an AFC model (DePaolo, 1981). The equation used is: $C_m = C^0_m F^{-z} + (r/r\text{-}1)\,(C_a/z)\,(1\text{-}F^{-z})$, with $z = (r + D\text{-}1)/(r\text{-}1)$. C_a and C_m are the concentrations in the contaminant and in the magma respectively. D corresponds to the bulk partition coefficient, F is the fraction of remaining melt and r is the ratio of assimilation rate to fractional crystallization rate. The compositions of the parental magma as the starting end member are chosen among the basalts with the highest MgO content (LO03 and LO15 for post- and pre-1960 groups, respectively). The crust underneath Lopevi is a likely contaminant composed of oceanic crust and of some former magmatic intrusives. However its precise composition remains unknown. An N-MORB trace element composition from Sun and McDonough (1989) is taken as representative of this crust. Values for the isotopic composition of the contaminant are chosen to obtain the best fit with our data set. These values are included into the isotopic composition range reported for the North Loyalty Basin by Briqueu and Lancelot (1983), Briqueu et al. (1994), and Peate et al. (1997), except for the Hf isotopic value which is significantly different from the single value reported by Pearce et al. (2007) and for the low $^{206}Pb/^{204}Pb$ value required for the recent contaminant. Assimilation of oceanic crust as partial melts (rather than bulk crust) is investigated. It has for main effect to increase the incompatible element concentration of the contaminant, while its Pb, Sr, Hf and Nd isotopic compositions remain unchanged. The trace element concentrations of the assimilated melts are calculated using a non-modal batch melting model (Shaw, 1970) of an N-MORB (Sun and McDonough, 1989) involving 1 and 10 % of melts, for the pre- and the post- 1960 contaminants, respectively.

Our model provides a good fit of the data in diagrams involving combined isotope ratios (insensitive to the fractional crystallization) or trace element and isotopic ratios (Fig. 9 and 10). Notably, the two distinct sets of C_a (with 1% and 10% of assimilated partial melts for pre- and post- 1960 lavas, respectively) and low (≤ 0.3) r parameters (Table 2) can account for the separate pre- and post- 1960 lava trends.

The pre-1960 lavas model requires a crustal partial melt contaminant with high U/Pb and Ba/Yb, associated with a low r, while the post-1960 model requires a contaminant with lower U/Pb, Ba/Yb ratios associated with a higher r value (Table 2). As seen in figures 9a and 9b, the post-1960 model requires a lower $^{206}Pb/^{204}Pb$ than needed for the pre-1960 lavas.

Ratios such as U/Pb and Ba/Yb (U and Ba being respectively more incompatible than Pb and Yb) are very sensitive to the degree of partial melting, while Sr-Nd-Pb-Hf isotopic ratios are not affected by this process and remain constant. Two distinct partial melting degrees (1% for pre- and 10% for post-1960 lavas) of a single N-MORB contaminant generate consistent C_a values for both series. Variable degrees of partial melting could be related to distinct conditions of pressure and temperature during assimilation or to a variable water content of the contaminant. The r values in the model for the post-1960 series are higher than those required for the older ones (0.3 versus 0.2), indicating a higher assimilation / fractional crystallization rate.

Many uncertainties remain in such models but our results are consistent with the model presented by Handley et al. (2008), with similar degrees of partial melting of the contaminant (1 and 10 % vs. 2-10 %), and r values (0.2 and 0.3 vs. 0.25). However we use a slightly more radiogenic Sr contaminant in our model (0.7033 vs. 0.7025) because a lower $^{87}Sr/^{86}Sr$ value cannot explain the pre-1960 variations.

5.3. Subduction component

5.3.1. Chemical time evolution

At the island arc scale, the Lopevi geochemical variations are limited (Monzier et al., 1997; Peate et al., 1997). Nevertheless at the scale of Lopevi volcano, differences appear between pre- and post-1960 lavas independently of the AFC process, especially when looking at trace element ratios such as Ba/Yb or Th/Nb (Figs. 6 and 10), as shown by the lack of overlap in Ba/Yb between both series (Fig. 10). The largest differences are observed in the most mafic (MgO rich) lavas, where the contamination effect is assumed to be the lowest and where the source signature is the most pronounced. Figure 11 shows the REE and trace element patterns of the basalts with MgO > 7 wt. %. Overall differences between both series are characterized by a higher enrichment in fluid mobile elements (Rb, Ba, U, K, Pb, Sr), in LREE (higher La/Yb) and in Th recorded in the post-1960 lavas. However the HFSE and HREE content are almost similar in the most mafic lavas (Fig. 11).

The isotopic signatures of Lopevi lavas are affected by the AFC process but the most mafic lavas from both series, which are supposed to be the least contaminated, have almost identical Nd, Pb and Hf isotopic compositions (Fig. 9). Only the Sr isotopes show a slight difference with more radiogenic ratios in the recent lavas.

5.3.2. Mantle source composition

Trace element variations in mafic lavas can reflect a change of 1) their mantle source mineralogy, 2) variable degrees of partial melting, or 3) different mantle sources. The most mafic post-1960 lavas have higher La/Yb ratios (~ 2.8 vs. 2.4) than the older ones (Fig. 11). As garnet incorporates some Yb amount in its structure, elevated La/Yb ratios in lavas could result from the melting of a garnet-bearing source at high pressure (Shimizu and Kushiro, 1975; Langmuir et al., 1977). However the observed differences between both series are moderate and cannot be attributed to a significant change in the mantle source mineralogy.

Changes in the partial melting degree of a single mantle source can also produce various trace element compositions in mafic magmas, in particular a fractionation between the most and the least incompatible elements. For example, while Nb is more incompatible than Yb during partial melting processes, pre- and post-1960 Lopevi lavas have identical Nb/Yb ratios (~ 0.6 for high-MgO basalts). Accordingly, partial melting cannot account for the chemical differences between the two series at Lopevi volcano.

In subduction zones, melting of the mantle wedge is triggered by the addition of a water-rich component released from the subducted oceanic lithosphere (e.g. Tatsumi, 1986; Peacock, 1990; Grove et al., 2006). This water-rich component carries trace elements into the mantle wedge and gives the typical enriched signature of arc magmas compared to MORB (McCulloch and Gamble, 1991). However its exact nature (aqueous fluids or hydrous melt) and origin (altered oceanic crust or sediments) remains largely debated (Elliott et al., 1997; Hawkesworth et al., 1997; Eiler et al., 1998; Prouteau et al., 2001). Lopevi lavas show Nb/Yb ratios similar to those found in MORB, indicating that the mantle in the subduction area was as depleted as the MORB mantle before the subduction component addition. Other trace element ratios involving fluid/melt mobile elements are higher than in MORB and document the element flux derived from the subducted plate. Among these elements, Ba and Pb are often used to indicate low T dehydration of the subducted lithosphere because they are highly mobile in hydrous fluids (Brenan et al., 1995; Stalder et al., 1998; Kessel et al., 2005) whereas Th is used as an indicator of sediment melting because Th/REE fractionation increases at high T when sediments melt (Johnson and Plank, 1999; Kessel et al., 2005; Plank, 2005; Hermann and Spandler, 2008).

Lopevi lavas are weakly enriched in incompatible elements compared to MORB which is consistent with a moderate modification of their mantle source by a subduction component. Th/La ratio is slightly higher than in MORB but the main enrichments affect Ba, Sr and Pb.

Even if the participation of a sediment melt cannot be ruled out, it is clear that low T dehydration fluids carried LILE into the Lopevi mantle source, in agreement with the high Ba/Yb and Pb/Ce ratios of the Lopevi lavas.

Post-1960 lavas are enriched in Ba and K while the less differentiated samples, which are also the less (or not at all) contaminated, have no significant differences in their Sr-Nd-Pb-Hf isotopic compositions. From these observations, one can argue that pre- and post-1960 lavas come from two different mantle sources beneath Lopevi. Both mantle portions have been metasomatised with fluids from a same origin, consistent with their identical isotopic composition, but the element flux was more elevated in the post-1960 mantle source, in agreement with the higher K and Ba enrichment observed in these more recent lavas.

5.4. Volcanological implications

Several eruptions have been recorded at Lopevi volcano between 1864 and 1939, before the volcano entered a period of quiescence for more than 20 years (Williams and Curtis, 1964). Volcanic activity resumed in 1960 by a large basaltic plinian eruption which forced a definitive evacuation of the people living on the island. This eruption marked the beginning of a new eruptive cycle of the volcano, with the production of mafic olivine-bearing magmas and the opening of the new lateral crater on the NW flank (Warden, 1967). During the following years the main crater was only active at the beginning of the eruptions while the main activity was concentrated in the new lateral cone or occurred along adjacent NW trending fissures. The onset of this new activity cycle in 1960 was accompanied by a shift in the trace element composition of the erupted magmas, as shown previously. The change occurred within a very short time scale (~ 20 years) while the deep processes of magma formation and evolution have been shown to appear on a larger time scale. Using the fractionation of Ra and Th in metasomatic fluids recorded by Ra-Th isotopes, Handley et al. (2008) estimated the metasomatism of the mantle wedge beneath Lopevi to have happened less than 8000 years ago, while the magmatic differentiation from basalt to basaltic andesite and the associated contamination was accomplished in less than 1000 years.

Taking these constraints all together indicates that fluid transfer from the subducted lithosphere into the mantle wedge creates mantle portions with different trace element compositions, probably in response to variable fluid flux in the mantle. Melting of at least two different mantle regions beneath Lopevi created magmas with slight differences in their trace element contents. These magmas followed different pathways from their source to the Lopevi volcano through the crust in which they were differentiated and contaminated in separate magma chambers beneath the volcano. The more enriched magma initiated the last volcanic cycle at Lopevi, and, following different pathways to the surface, created a new emission centre on the flank of the volcano.

The very short time scale of this shift indicates that the “older’ and less enriched magma is still present beneath the volcano and can erupt again from the summit crater in the years or decades to come.

6. Conclusions

- New sampling of the Lopevi island increases the previous data set (mainly post-1960) of Handley et al. (2008), providing insight into the older history of the volcano. Notably, the pre-1960 data set contains more differentiated rocks, up to 61 wt % SiO_2.
- Chemical and isotopic data on pre- and post-1960 lavas confirm the contamination of the ascending magmas by partial melts derived from the oceanic crust beneath the volcano. AFC

modelling requires 1% and 10% of assimilated crustal melts to account for the pre- and post-1960 lavas, respectively.

- Pre- and post-1960 lavas show different trace element compositions but very similar isotopic ratios. These differences, unrelated to the contamination process, are ascribed to the partial melting of different portions of the mantle, which have undergone slightly different metasomatic fluid flux from the subducted oceanic lithosphere.
- The renewal of volcanic activity in 1960, after more than 20 years of quiescence, marks the involvement of a new batch of magma coming from a different mantle source. However, the contrasted time scales involved in the magma genesis at depth and the volcanological evolution at the surface imply that the old magma is still present beneath the volcano but so far unable to mix with the younger one.

Acknowledgments

We thank the Pole Spectrometry Ocean (Emmanuel Ponzevera, Phillipe Nonotte, Claire Bassoullet, Céline Liorzou), Bleuenn Gueguen and Shasa Labanieh for their help to the data acquisition. Paul Capiez is acknowledged for XRF analyses. This work was supported by the ANR contract Arc-Vanuatu led by Bernard Pelletier. Esline Garaebiti and the people from the Vanuatu Geohazards Observatory are warmly thanked for their help during the field trips. We also thank the two reviewers for their valuable comments.

Figure captions

Figure 1: (a) Bathymetric map of the Vanuatu island arc. Inset: General map of the south-west Pacific. (b) Interpretative map of the Vanuatu islands showing the general tectonic setting adapted from Pelletier et al. (1998). The Back Arc Thrust Belt is the thrusting of the Eastern belt on the North Fiji Basin (Calmant et al., 2003). The Vanuatu active arc (central chain) is drawn in red, with small white triangles representing the active volcanoes. Inclined hatching is used for islands belonging to the Western belt and to the Eastern belt. Simple arrows indicate the convergent rate in $cm.a^{-1}$ of the subducted plate from GPS data (Calmant et al., 2003). Double arrows represent the divergent rates in $cm.a^{-1}$ in the back arc domain (Price and Kroenke, 1991; Auzende et al., 1994; Huchon et al., 1994; Pelletier et al., 1998). The associated thin lines show the active spreading axes. Brown areas represent ridges and plateaus (submarine relief) on the subducted plate. Dashed bold lines represent the major faults and the associated half arrows represent the movement of each block. The dotted line in the north represents the ancient Vitiaz trench lineament. The star indicates the location of the DSDP (Deep Sea Drilling Project) hole 286.

Figure 2: (a) Location map of Lopevi samples (circles), and the main recent lava flows, adapted from Handley et al. (2008). Circles represent the location of the samples from this work, whereas triangles represent those studied by Handley et al. (2008). (b) Regional bathymetric map of the central part of the Vanuatu arc, with the location of the Lopevi island.

Figure 3: K_2O versus SiO_2 diagram (Peccerillo and Taylor, 1976) illustrating the compositional diversity of the Lopevi lavas emitted before and after 1960, and the overall dominance of basic compositions for the Vanuatu lavas (small circles: data from Georoc database and from our unpublished data. Triangles are used for data from Handley et al.

(2008). Lopevi lavas plot in the medium-K calc alkaline series with low K_2O content compared to other Vanuatu lavas.

Figure 4: Major element binary diagrams showing the effect of fractional crystallization with crystallization of olivine and clinopyroxene before plagioclase. (a) MgO and (b) Al_2O_3 shown as a function of silica content.

Figure 5: (a) REE patterns of the Lopevi lavas normalized to the chondritic values from McDonough and Sun (1995). (b) Extended trace elements patterns of Lopevi lavas normalized to the N-MORB values from Sun and McDonough (1989). Only samples measured with the method described by Chauvel et al. (2011) are shown in the extended diagram. Shaded areas correspond to Vanuatu basalts reported by Peate et al. (1997) from islands facing the D'Entrecasteaux Ridge (DER) collision (e.g. Gaua, Aoba, Ambrym).

Figure 6: Nb versus Th diagram showing the behaviour of two highly incompatible elements with similar bulk D values. Pre- (gray line) and post-1960 (black line) lavas display different Th/Nb ratios.

Figure 7: Isotopic diagrams showing the very restricted range of variation of the Lopevi lavas. (a) Nd-Sr isotope diagram. The mantle array is from Hofmann and White (1982). (b) Hf-Nd isotope diagram. The global correlation is from Graham et al. (2006). (c) $^{208}Pb/^{204}Pb$- $^{206}Pb/^{204}Pb$ and (d) $^{207}Pb/^{204}Pb$ - $^{206}Pb/^{204}Pb$ diagrams. The Northern Hemisphere Reference Line is from Hart (1984). The discrimination line is from Pearce et al. (2007) in diagram (b) and from Kempton et al. (2002) in diagram (c). MORB data are from Meyzen et al. (2007), using the East Pacific Rise data for the Pacific MORB and the South East Indian Ridge data

for the Indian MORB (excluding the references from the Australia Antarctica Discordance). NLB AOC: Altered Oceanic Crust from the North Loyalty Basin. NLB Sediments: North Loyalty Basin sediments. NLB data correspond to samples coming from the DSDP Hole 286 (Fig. 1) and are from Peate et al. (1997)(for Pb, samples leached), Briqueu et al. (1994)(for Sr-Nd-Pb) and from Pearce et al. (2007)(for Sr-Nd-Hf). Vanuatu data are from Peate et al. (1997), Laporte et al. (1998), Turner et al. (1999), Pearce et al. (2007), and from personal unpublished data.

Figure 8: (a) $^{87}Sr/^{86}Sr$ (b) $^{143}Nd/^{144}Nd$ (c) $^{208}Pb/^{204}Pb$ ratios versus SiO_2 wt % diagrams showing the decrease (Sr, Pb) and the increase (Nd) of the isotopic ratios during the magmatic differentiation (SiO_2 as an index of differentiation) due to crustal contamination. 2σ represents the mean of the individual analytical error.

Figure 9: (a) $^{206}Pb/^{204}Pb$ vs. U/Pb (b) $^{207}Pb/^{204}Pb$ vs. $^{206}Pb/^{204}Pb$ (c) $^{176}Hf/^{177}Hf$ vs. $^{208}Pb/^{204}Pb$ diagrams showing combined assimilation and fractional crystallization (AFC) models described in the text. The starting end-members are the high MgO basalts LO03 (post-1960) and LO15 (pre-1960). The fraction of melt remaining (F) is indicated on the AFC model curves by tick marks every 0.1 step. Parameters used in the models for the pre- 1960 (gray curve) and the post- 1960 (black curve) are reported in the Table 2.

Figure 10: $^{87}Sr/^{86}Sr$ versus Ba/Yb diagram showing the geochemical differences between the pre- and the post-1960 lavas, especially for the less differentiated samples, and the effect of AFC processes (parameters of the model in Table 2).

Figure 11: Extended trace element patterns showing the major differences between the high MgO basalts LO03, LO04 (post-1960) and LO15 and LO20 (pre-1960). REE in bold characters. Inset: REE patterns normalized to the chondritic values from McDonough and Sun (1995). Boxes indicate elements showing significant difference between the two series.

Table 1: Major elements are presented on a volatile-free basis to 100 % with total iron as Fe_2O_3(t). Samples ticked with a " §" were measured using the protocole developed by Barrat et al. (1996), while the others were measured by the protocole described in Chauvel et al. (2011). LO04 was measured by both protocols and standard deviation (sd) values between the two measurements are given. Sr isotopic data measured on a Finnigan MAT26X for data ticked with a "*", and on a Thermo Fischer TRITON for others.

Table 2: AFC model parameters and results of batch melting model. The trace element contents of the contaminant (C_a) were calculated from the batch melting (1 % for the pre-1960 group and 10 % for the post- 1960 group) of a metabasalt (source mineralogy: 0.2 orthopyroxene, 0.40 clinopyroxene, 0.25 plagioclase, 0.15 amphibole) having the trace element content of an N-MORB from Sun and McDonough (1989). The respective contributions to the melt are 0.4 clinopyroxene, 0.35 amphibole, 0.2 plagioclase, 0.05 orthopyroxene. Partition coefficients used to calculate bulk D values are from Adam and Green (2006) and Aignertorres et al. (2007). Partition coefficient of Yb between clinopyroxene and melt is from Green et al. (2000). Partition coefficients of Pb are from Hauri et al. (1994), Bindeman et al. (1998), and McKenzie and O'Nions (1991). The isotopic ratios of the contaminant (R_a) were chosen to fit correctly the data and are consistent with values found in MORB. "r" value used is 0.3 for the post-1960 lavas and 0.2 for the pre-1960 lavas. D, Ca, and r are assumed to be constant during the AFC process. The r value used is as low as

possible, because a small degree of contamination is easier to invoke. The starting end-members are the high MgO basalts LO03 (post-1960) and LO15 (pre-1960). Parameters used in the model are slightly different between the pre- and the post-1960 lavas.

References

Adam, J. and Green, T., 2006. Trace element partitioning between mica- and amphibole-bearing garnet lherzolite and hydrous basanitic melt: 1. Experimental results and the investigation of controls on partitioning behaviour. Contributions to Mineralogy and Petrology, 152(1): 1-17.

Aigner-Torres, M., Blundy, J., Ulmer, P. and Pettke, T., 2007. Laser Ablation ICPMS study of trace element partitioning between plagioclase and basaltic melts: an experimental approach. Contributions to Mineralogy and Petrology, 153(6): 647-667.

Andrew, J.E., Packham, G., Eade, J.V., Holdsworth, B.K., Jones, D.L., De Vriesklein, G., Kroenke, L.W., Saito, T., Shafik, S., Stoeser, D.B. and Van Der Lingen, G.J., 1973. Site 285 and 286. In: Andrew, J.E. and Packham, G. (Eds.), Initial reports of the Deep Sea Drilling Project, Washington, DC, United States (USA), pp. 27-131.

Auzende, J.M., Pelletier, B. and Eissen, J.P., 1995. The North Fiji Basin: Geology, Structure and geodynamic evolution. In: Taylor, B. (Ed.), Back-arc basin: tectonics and magmatism, New York, pp. 139-175.

Auzende, J.M., Pelletier, B. and Lafoy, Y., 1994. Twin active spreading ridges in the North Fiji Basin (Southwest Pacific). Geology, 22(1): 63-66.

Baker, P.E. and Condliffe, E., 1996. Compositional variations in submarine volcanic ashes from the vicinity of the Vanuatu island arc: A response to ridge-arc collision? Journal of Volcanology and Geothermal Research, 72(3-4): 225-238.

Barrat, J.A., Keller, F., Amosse, J., Taylor, R.N., Nesbitt, R.W. and Hirata, T., 1996. Determination of rare earth elements in sixteen silicate reference samples by ICP-MS after Tm addition and ion exchange separation. Geostandards Newsletter, 20(1): 133-139.

Barsdell, M., 1988. Petrology and petrogenesis of clinopyroxene-rich tholeiitic lavas, Merelava volcano, Vanuatu. Journal of Petrology, 29(5): 927-964.

Barsdell, M. and Berry, R.F., 1990. Origin and evolution of primitive island-arc ankaramites from Western Epi, Vanuatu. Journal of Petrology, 31(3): 747-777.

Barsdell, M., Smith, I.E.M. and Spoerli, K.B., 1982. The origin of reversed geochemical zoning in the northern New Hebrides volcanic arc. Contributions to Mineralogy and Petrology, 81(2): 148-155.

Bindeman, I.N., Davis, A.M. and Drake, M.J., 1998. Ion microprobe study of plagioclase-basalt partition experiments at natural concentration levels of trace elements. Geochimica et Cosmochimica Acta, 62(7): 1175-1193.

Brenan, J.M., Shaw, H.F., Ryerson, F.J. and Phinney, D.L., 1995. Mineral-aqueous fluid partitioning of trace-elements at 900 degrees-C and 2.0 gpa - Constraints on the trace-element chemistry of mantle and deep-crustal fluids. Geochimica et Cosmochimica Acta, 59(16): 3331-3350.

Briqueu, L. and Lancelot, J.R., 1983. Sr isotopes and K, Rb, Sr balance in sediments and igneous rocks from the subducted plate of the Vanuatu (New Hebrides) active margin. Geochimica et Cosmochimica Acta, 47: 191-200.

Briqueu, L., Laporte, C., Crawford, A.J., Hasenaka, T., Baker, P.E. and Coltorti, M., 1994. Temporal magmatic evolution of the Aoba Basin, central New Hebrides island arc; Pb, Sr, and Nd isotopic evidence for the coexistence of two mantle components beneath the arc. In: Greene, H.G., Collot, J.-Y., Stokking, L.B. et al. (Eds.), Proceedings of the Ocean Drilling Program, Scientific Results, 134, College Station, TX, United States (USA), pp. 393-401.

Bryan, W.B., Finger, L.W. and Chayes, F., 1969. Estimating proportions in petrographic mixing equations by least-squares approximation. Science, 163(3870): 926-927.

Calmant, S., Pelletier, B., Lebellegard, P., Bevis, M., Taylor, F.W. and Phillips, D.A., 2003. New insights on the tectonics along the New Hebrides subduction zone based on GPS results. Journal of Geophysical Research-Solid Earth, 108(B6): 2319–2340.

Châtelain, J.L., Molnar, P., Prévot, R. and Isacks, B., 1992. Detachment of part of the downgoing slab and uplift of the New Hebrides (Vanuatu) islands. Geophysical Research Letters, 19(14): 1507-1510.

Chauvel, C., Bureau, S. and Poggi, C., 2011. Comprehensive Chemical and Isotopic Analyses of Basalt and Sediment Reference Materials. Geostandards and Geoanalytical Research, 35(1): 125-143.

Collot, J.Y., Daniel, J. and Burne, R.V., 1985. Recent tectonics associated with the subduction collision of the d'Entrecasteaux zone in the central New-Hebrides. Tectonophysics, 112(1-4): 325-356.

Crawford, A.J., Briqueu, L., Laporte, C. and Hasenaka, T., 1995. Coexistence of Indian and Pacific oceanic upper mantle reservoirs beneath the central New Hebrides island arc. In: Taylor, B. and Natland, J. (Eds.), Active margins and marginal basins of the western Pacific. Geophysical Monograph. American Geophysical Union, Washington, DC, United States (USA), pp. 199–217.

DePaolo, D.J., 1981. Trace-element and isotopic effects of combined wallrock assimilation and fractional crystallization. Earth and Planetary Science Letters, 53(2): 189-202.

Dupuy, C., Dostal, J., Marcelot, G., Bougault, H., Joron, J.L. and Treuil, M., 1982. Geochemistry of basalts from central and southern New Hebrides arc - Implication for their source rock composition. Earth and Planetary Science Letters, 60(2): 207-225.

Eggins, S.M., 1993. Origin and differentiation of picritic arc magmas, Ambae (Aoba), Vanuatu. Contributions to Mineralogy and Petrology, 114(1): 79-100.

Eiler, J.M., McInnes, B., Valley, J.W., Graham, C.M. and Stolper, E.M., 1998. Oxygen isotope evidence for slab-derived fluids in the sub-arc mantle. Nature, 393(6687): 777-781.

Elliott, T., Plank, T., Zindler, A., White, W. and Bourdon, B., 1997. Element transport from slab to volcanic front at the Mariana arc. Journal of Geophysical Research-Solid Earth, 102(B7): 14991-15019.

Galer, S.J.G. and Abouchami, W., 1998. Practical application of lead triple spiking for correction of instrumental mass discrimination, Goldschmidt conference, Toulouse, pp. 491-492.

Graham, D.W., Blichert-Toft, J., Russo, C.J., Rubin, K.H. and Albarède, F., 2006. Cryptic striations in the upper mantle revealed by hafnium isotopes in southeast Indian ridge basalts. Nature, 440(7081): 199-202.

Green, T.H., Blundy, J.D., Adam, J. and Yaxley, G.M., 2000. SIMS determination of trace element partition coefficients between garnet, clinopyroxene and hydrous basaltic liquids at 2-7.5 GPa and 1080-1200 degrees C. Lithos, 53(3-4): 165-187.

Greene, H.G., Collot, J.-Y., Fisher, M.A. and Crawford, A.J., 1994. Neogene tectonic evolution of the New Hebrides island arc; a review incorporating ODP drilling results. In: Greene, H.G., Collot, J.-Y., Stokking, L.B. and al., e. (Eds.), Proceedings of the

Ocean Drilling Program, Scientific Results, 134, College Station, TX, United States (USA), pp. 19-46.

Greene, H.G., MacFarlane, A., Johnson, D.P. and Crawford, A.J., 1988. Structure and tectonics of the central New Hebrides arc. In: Greene, H.G. and Wong, F.L. (Eds.), Geology and offshore resources of Pacific Island Arcs - Vanuatu region. Earth Science Series. Circum-Pacific Council for Energy and Mineral Resources, Houston, TX, United States (USA), pp. 377-412.

Grove, T.L., Chatterjee, N., Parman, S.W. and Medard, E., 2006. The influence of H2O on mantle wedge melting. Earth and Planetary Science Letters, 249(1-2): 74-89.

Handley, H.K., Turner, S.P., Smith, I.E.M., Stewart, R.B. and Cronin, S.J., 2008. Rapid timescales of differentiation and evidence for crustal contamination at intra-oceanic arcs: Geochemical and U-Th-Ra-Sr-Nd isotopic constraints from Lopevi Volcano, Vanuatu, SW Pacific. Earth and Planetary Science Letters, 273(1-2): 184-194.

Hart, S.R., 1984. A large-scale isotope anomaly in the Southern-Hemisphere mantle. Nature, 309(5971): 753-757.

Hauri, E.H., Wagner, T.P. and Grove, T.L., 1994. Experimental and natural partitioning of Th, U, Pb and other trace-elements between garnet, clinopyroxene and basaltic melts. Chemical Geology, 117(1-4): 149-166.

Hawkesworth, C.J., Turner, S.P., McDermott, F., Peate, D.W. and vanCalsteren, P., 1997. U-Th isotopes in arc magmas: Implications for element transfer from the subducted crust. Science, 276(5312): 551-555.

Hermann, J. and Spandler, C.J., 2008. Sediment melts at sub-arc depths: An experimental study. Journal of Petrology, 49(4): 717-740.

Heyworth, Z., Knesel, K.M., Turner, S.P. and Arculus, R.J., 2011. Pb-isotopic evidence for rapid trench-parallel mantle flow beneath Vanuatu. Journal of the Geological Society, 168(1): 265-271.

Hildreth, W. and Moorbath, S., 1988. Crustal contributions to arc magmatism in the Andes of Central Chile. Contributions to Mineralogy and Petrology, 98(4): 455-489.

Hofmann, A.W. and White, W.M., 1982. Mantle plume from ancient oceanic-crust. Earth and Planetary Science Letters, 57(2): 421-436.

Huchon, P., Gracia, E., Ruellan, E., Joshima, M. and Auzende, J.M., 1994. Kinematics of active spreading in the central North Fiji Basin (Southwest Pacific). Marine Geology, 116(1-2): 69-87.

Jochum, K.P. and Brueckner, S.M., 2008. Reference Materials in Geoanalytical and Environmental Research - Review for 2006 and 2007. Geostandards and Geoanalytical Research, 32(4): 405-452.

Johnson, M.C. and Plank, T., 1999. Dehydration and melting experiments constrain the fate of subducted sediments. Geochemistry Geophysics Geosystems, 1. http://dx.doi.org/10.1029/1999GC000014

Kempton, P.D., Pearce, J.A., Barry, T.L., Fitton, J.G., Langmuir, C. and Christie, D.M., 2002. Sr-Nd-Pb-Hf isotope results from ODP Leg 187: Evidence for mantle dynamics of the Australian-Antarctic Discordance and origin of the Indian MORB source. Geochemistry Geophysics Geosystems, 3. http://dx.doi.org/10.1029/2002GC000320

Kessel, R., Schmidt, M.W., Ulmer, P. and Pettke, T., 2005. Trace element signature of subduction-zone fluids, melts and supercritical liquids at 120-180 km depth. Nature, 437(7059): 724-727.

Langmuir, C.H., Bender, J.F., Bence, A.E., Hanson, G.N. and Taylor, S.R., 1977. Petrogenesis of basalts from Famous area - Mid-Atlantic Ridge. Earth and Planetary Science Letters, 36(1): 133-156.

Laporte, C., Briqueu, L., Cluzel, D. and Eissen, J.P., 1998. Isotopic gradient along the New Hebrides arc (Vanuatu, SW Pacific). Collision of the d'Entrecasteaux Zone and heterogeneity of mantle sources. Comptes Rendus de l'Académie des Sciences Série IIA, 326(2): 101-106.

MacFarlane, A., Carney, J.N., Crawford, A.J. and Greene, H.G., 1988. Vanuatu - A review of the onshore geology. In: Greene, H.G., Wong, F.L. (Ed.), Geology and offshore resources of Pacific Island Arcs - Vanuatu region. Earth Science Series. Circum-Pacific Council for Energy and Mineral Resources, Houston, TX, United States (USA), pp. 24-68.

Manhès, G., Allègre, C.J. and Provost, A., 1984. U-Th-Pb systematics of the eucrite Juvinas - Precise age-determination and evidence for exotic lead. Geochimica et Cosmochimica Acta, 48(11): 2247-2264.

Mann, P. and Taira, A., 2004. Global tectonic significance of the Solomon Islands and Ontong Java Plateau convergent zone. Tectonophysics, 389(3-4): 137-190.

McCulloch, M.T. and Gamble, J.A., 1991. Geochemical and geodynamical constraints on subduction zone magmatism. Earth and Planetary Science Letters, 102(3-4): 358-374.

McDonough, W.F. and Sun, S.S., 1995. The composition of the Earth. Chemical Geology, 120(3-4): 223-253.

McKenzie, D. and O'Nions, R.K., 1991. Partial melt distributions from inversion of Rare-Earth Element concentrations. Journal of Petrology, 33(6): 1453-1453.

Meffre, S. and Crawford, A.J., 2001. Collision tectonics in the New Hebrides arc (Vanuatu). Island Arc, 10(1): 33-50.

Métrich, N., Allard, P., Aiuppa, A., Bani, P., Bertagnini, A., Shinohara, H., Parello, F., Di Muro, A., Garaebiti, E., Belhadj, O. and Massare, D., 2011. Magma and Volatile Supply to Post-collapse Volcanism and Block Resurgence in Siwi Caldera (Tanna Island, Vanuatu Arc). Journal of Petrology, 52(6): 1077-1105.

Meyzen, C.M., Blichert-Toft, J., Ludden, J.N., Humler, E., Mevel, C. and Albarède, F., 2007. Isotopic portrayal of the Earth's upper mantle flow field. Nature, 447(7148): 1069-1074.

Monzier, M., Danyushevsky, L.V., Crawford, A.J., Bellon, H. and Cotten, J., 1993. High-Mg andesites from the southern termination of the New-Hebrides island-arc (SW Pacific). Journal of Volcanology and Geothermal Research, 57(3-4): 193-217.

Monzier, M., Robin, C., Eissen, J.P. and Cotten, J., 1997. Geochemistry vs. seismo-tectonics along the volcanic New Hebrides Central Chain (Southwest Pacific). Journal of Volcanology and Geothermal Research, 78(1-2): 1-29.

Pascal, G., Isacks, B.L., Baranzangi, M. and Dubois, J., 1978. Precise relocalisations of earthquakes and seismotectonics of the New Hebrides island arc. Journal of Geophysical Research, 83: 4957-4973.

Peacock, S.M., 1990. Fluid processes in subduction zones. Science, 248(4953): 329-337.

Pearce, J.A., Kempton, P.D. and Gill, J.B., 2007. Hf-Nd evidence for the origin and distribution of mantle domains in the SW Pacific. Earth and Planetary Science Letters, 260(1-2): p 98-114.

Peate, D.W., Baker, J.A., Jakobsson, S.P., Waight, T.E., Kent, A.J.R., Grassineau, N.V. and Skovgaard, A.C., 2009. Historic magmatism on the Reykjanes Peninsula, Iceland: a snap-shot of melt generation at a ridge segment. Contributions to Mineralogy and Petrology, 157(3): 359-382.

Peate, D.W., Pearce, J.A., Hawkesworth, C.J., Colley, H., Edwards, C.M.H. and Hirose, K., 1997. Geochemical variations in Vanuatu arc lavas: the role of subducted material and a variable mantle wedge composition. Journal of Petrology, 38(10): 1331-1358.

Peccerillo, A. and Taylor, S.R., 1976. Geochemistry of Eocene calc-alkaline volcanic-rocks from Kastamonu area, Northern Turkey. Contributions to Mineralogy and Petrology, 58(1): 63-81.

Pelletier, B., Calmant, S. and Pillet, R., 1998. Current tectonics of the Tonga New Hebrides region. Earth and Planetary Science Letters, 164(1-2): 263-276.

Picard, C., Monzier, M., Eissen, J.-P. and Robin, C., 1995. Concomitant evolution of tectonic environment and magma geochemistry, Ambrym volcano (Vanuatu, New Hebrides arc). In: Smellie, J.L. (Ed.), Volcanism associated with extension at consuming plate margin. Geological Society of America, Special Publication, pp. 135-154.

Plank, T., 2005. Constraints from thorium/lanthanum on sediment recycling at subduction zones and the evolution of the continents. Journal of Petrology, 46(5): 921-944.

Price, R.C. and Kroenke, L.W., 1991. Tectonics and magma genesis in the northern North Fiji Basin. Marine Geology, 98(2-4): 241-258.

Prouteau, G., Scaillet, B., Pichavant, M. and Maury, R., 2001. Evidence for mantle metasomatism by hydrous silicic melts derived from subducted oceanic crust. Nature, 410(6825): 197-200.

Raos, A.M. and Crawford, A.J., 2004. Basalts from the Efate Island Group, central section of the Vanuatu arc, SW Pacific: geochemistry and petrogenesis. Journal of Volcanology and Geothermal Research, 134(1-2): 35-56.

Richard, P., Shimizu, N. and Allègre, C.J., 1976. Nd143/Nd146 A natural tracer - Application to oceanic basalt. Earth and Planetary Science Letters, 31(2): 269-278.

Shaw, D.M., 1970. Trace element fractionation during anatexis. Geochimica et Cosmochimica Acta, 34(2): 237-243.

Shimizu, N. and Kushiro, I., 1975. Partitioning of rare-earth elements between garnet and liquid at high-pressures - Preliminary experiments. Geophysical Research Letters, 2(10): 413-416.

Sorbadere, F., Schiano, P., Métrich, N. and Garaebiti, E., 2011. Insights into the origin of primitive silica-undersaturated arc magmas of Aoba volcano (Vanuatu arc). Contributions to Mineralogy and Petrology, 162(5): 995-1009.

Stalder, R., Foley, S.F., Brey, G.P. and Horn, I., 1998. Mineral aqueous fluid partitioning of trace elements at 900-1200 degrees C and 3.0-5.7 GPa: New experimental data for garnet, clinopyroxene, and rutile, and implications for mantle metasomatism. Geochimica et Cosmochimica Acta, 62(10): 1781-1801.

Sun, S.S. and McDonough, W.F., 1989. Chemical and isotopic systematics of oceanic basalts: Implications for mantle composition and processes, Chemical and isotopic systematics of oceanic basalts. Geological Society, London, Special Publications., pp. 313-345.

Tatsumi, Y., 1986. Formation of the volcanic front in subduction zones. Geophysical Research Letters, 13(8): 717-720.

Taylor, F.W., Baevis, M.G., Schutz, B.E., Kuang, D., Recy, J., Calmant, S., Charley, D., Regnier, M., Perin, B., Jackson, M. and Reichenfeld, C., 1995. Geodetic measurements of convergence at the New-Hebrides-island arc indicate arc fragmentation caused by an impinging aseismic ridge. Geology, 23(11): 1011-1014.

Turner, S.P., Peate, D.W., Hawkesworth, C.J., Eggins, S.M. and Crawford, A.J., 1999. Two mantle domains and the time scales of fluid transfer beneath the Vanuatu arc. Geology, 27(11): 963-966.

Warden, A.J., 1967. The 1963–65 eruption of Lopevi Volcano (New Hebrides). Bulletin of volcanology, 30: 277-306.

White, W.M., Albarède, F. and Telouk, P., 2000. High-precision analysis of Pb isotope ratios by multi-collector ICP-MS. Chemical Geology, 167(3-4): 257-270.

Williams, C.E. and Curtis, R., 1964. The eruption of Lopevi, New Hebrides, July 1960. Bulletin of volcanology, 27: 423-433.

Woodhead, J.D., 1989. Geochemistry of the mariana arc (Western Pacific) - Source composition and processes. Chemical Geology, 76(1-2): 1-24.

Yang, Y.H., Zhang, H.F., Chu, Z.Y., Xie, L.W. and Wu, F.Y., 2010. Combined chemical separation of Lu, Hf, Rb, Sr, Sm and Nd from a single rock digest and precise and accurate isotope determinations of Lu-Hf, Rb-Sr and Sm-Nd isotope systems using Multi-Collector ICP-MS and TIMS. Int. J. Mass Spectrom., 290(2-3): 120-126.

Table 1

Click here to download Table: Table1-data.pdf

Table 1: Isotope ratios, major and trace element content for the Lopevi lavas

Post-1960 lavas

	LO01	LO02	LO03	LO04	LO05	LO06	LO07	LO17	LO25	LO30	LO31	LO35
Rock type	lava flow	lava flow	lava flow	lava islet	lava flow	bomb	scoria	lava flow	lava flow	bomb	lava flow	block
Age	2001	1963	2000	1960 ?	2003	post-2003	post-2003	2004-2005	2000	?	2000	1968 ?
Latitude	S 16° 30' 56.7"	S 16° 30' 51.3"	S 16° 31' 01.3"	S 16° 30' 38.0"	S 16° 29' 54.4"	S 16° 29' 57.9"	S 16° 29' 57.9"	S 16° 31' 53.7"	S 16° 30' 42.0"	S 16° 30' 30.6"	S 16° 30' 44.3"	S 16° 31' 05.8"
Longitude	E 168° 18' 51.0"	E 168° 18' 50.8"	E 168° 18' 53.3"	E 168° 18' 46.7"	E 168° 18' 55.1"	E 168° 19' 11.6"	E 168° 19' 11.6"	E 168° 19' 55.3"	E 168° 19' 45.8"	E 168° 20' 23.2"	E 168° 19' 16.4"	E 168° 21' 00.6"
wt %												
SiO_2	52,01	50,71	49,57	49,56	50,60	50,68	50,65	51,15	51,03	51,95	52,45	53,62
TiO_2	0,79	0,73	0,69	0,70	0,73	0,72	0,72	0,75	0,76	0,76	0,82	0,84
Al_2O_3	18,79	19,32	16,33	16,25	19,46	19,60	19,66	19,15	19,58	17,26	18,71	17,04
Fe_2O_3 (t)	9,51	9,56	10,48	10,62	9,54	9,49	9,41	9,52	9,46	9,97	9,44	9,87
MnO	0,16	0,16	0,18	0,17	0,16	0,16	0,15	0,16	0,16	0,17	0,16	0,17
MgO	4,38	4,67	7,68	7,77	4,66	4,56	4,49	4,58	4,41	5,79	4,34	4,90
CaO	10,54	11,46	12,13	11,95	11,46	11,45	11,53	11,11	11,12	10,48	10,18	9,37
Na_2O	2,74	2,54	2,10	2,13	2,54	2,49	2,49	2,61	2,58	2,64	2,81	2,96
K_2O	0,89	0,70	0,69	0,69	0,70	0,70	0,75	0,80	0,74	0,80	0,92	1,02
P_2O_5	0,18	0,15	0,15	0,15	0,15	0,15	0,15	0,17	0,16	0,17	0,19	0,21
LOI	-0,42	-0,43	-0,49	-0,48	-0,48	-0,52	-0,39	-0,48	0,01	-0,39	-0,39	-0,35
Total	100,73	100,94	101,05	100,92	100,97	100,7	100,59	100,95	100,07	100,69	100,54	100,68
ppm												
Sc	29	29	35	36	28	30	29	30	28	36	27	30
V	256	265	277	274	269	262	266	265	277	274	266	259
Cr	28	26	190	188	28	31	31	34	17	63	27	45
Co	27	29	40	40	29	29	28	29	26	31	23	27
Ni	17	17	56	61	19	19	19	20	17	27	16	20
Cu	128	122	115	115	121	135	115	125	114	99	106	119
Ga	18	19	16	17	17	19	18	18	18	15	18	19
Rb	15,7	12,4	12,4	12,4	12,1	12,2	12,0	14,3	12,6	14,1	15,4	16,6
Sr	340	366	359	360	365	368	365	363	374	311	331	304
Y	23,6	19,9	17,4	17,5	19,7	19,7	19,2	21,2	19,2	21,9	23,6	25,1
Zr	74	56	47	49	56	57	55	65	56	68	76	89
Nb	1,81	1,38	1,11	1,18	1,38	1,38	1,35	1,55	1,40	1,69	1,85	2,18
Cs	0,40	0,33	0,36	0,37	0,32	0,32	0,32	0,38	0,34	0,38	0,42	0,45
Ba	164	140	135	138	141	139	138	155	141	159	165	178
La	6,99	5,51	4,98	5,21	5,50	5,52	5,39	6,38	5,56	6,34	7,07	7,80
Ce	16,0	12,9	11,7	12,2	12,9	12,8	12,4	14,6	12,8	14,9	16,2	18,4
Pr	2,34	1,90	1,77	1,84	1,89	1,90	1,83	2,11	1,91	2,14	2,37	2,63
Nd	10,9	9,1	8,7	8,9	9,0	9,0	8,8	10,0	9,1	10,2	11,2	12,4
Sm	3,04	2,55	2,42	2,46	2,53	2,53	2,49	2,77	2,58	2,83	3,09	3,36
Eu	0,99	0,88	0,83	0,85	0,87	0,88	0,86	0,93	0,87	0,94	1,00	1,06
Gd	3,52	2,97	2,79	2,84	2,96	2,95	2,87	3,20	2,91	3,34	3,54	3,82
Tb	0,58	0,50	0,46	0,46	0,49	0,49	0,48	0,53	0,49	0,56	0,60	0,63
Dy	3,89	3,31	2,95	3,06	3,28	3,28	3,25	3,54	3,23	3,74	3,99	4,24
Ho	0,83	0,70	0,63	0,65	0,70	0,70	0,69	0,75	0,70	0,79	0,84	0,91
Er	2,50	2,10	1,86	1,89	2,09	2,10	2,06	2,25	2,08	2,35	2,54	2,71
Yb	2,43	2,03	1,78	1,82	2,01	2,01	1,98	2,17	2,03	2,31	2,49	2,62
Lu	0,36	0,31	0,27	0,27	0,30	0,30	0,30	0,33	0,31	0,35	0,37	0,40
Hf	2,03	1,59	1,35	1,40	1,59	1,57	1,56	1,79	1,61	1,87	2,12	2,42
Ta	0,113	0,085	0,071	0,074	0,087	0,087	0,085	0,098	0,090	0,108	0,120	0,141
Pb	3,16	2,60	2,62	2,54	2,58	2,62	2,76	2,96	2,79	1,98	1,46	3,91
Th	0,91	0,72	0,62	0,64	0,71	0,71	0,71	0,83	0,77	0,82	0,95	1,02
U	0,38	0,29	0,26	0,26	0,29	0,29	0,29	0,34	0,32	0,35	0,39	0,45
Isotopes												
$^{87}Sr/^{86}Sr$	0.703970 ± 11 *	0.703996 ± 8 *	0.704035 ± 9 *	0.704085 ± 8	0.703969 ± 9 *			0.704011 ± 10 *				0.704012 ± 8
$^{143}Nd/^{144}Nd$	0.51298 ± 6	0.512968 ± 6	0.512975 ± 6	0.512971 ± 6	0.512968 ± 6			0.512961 ± 10				0.512986 ± 8
εNd	6,67	6,44	6,57	6,50	6,44			6,30				6,79
$^{206}Pb/^{204}Pb$	18.448 ± 1	18.444 ± 1	18.512 ± 1	18.508 ± 1	18.447 ± 1			18.453 ± 1				18.471 ± 1
$^{207}Pb/^{204}Pb$	15.538 ± 1	15.543 ± 1	15.549 ± 1	15.547 ± 1	15.542 ± 1			15.541 ± 1				15.543 ± 1
$^{208}Pb/^{204}Pb$	38.379 ± 3	38.396 ± 2	38.425 ± 3	38.422 ± 3	38.397 ± 2			38.392 ± 2				38.394 ± 2
$^{176}Hf/^{177}Hf$	0.283183 ± 3	0.283179 ± 4	0.283174 ± 4	0.28317 ± 3	0.283157 ± 10			0.283184 ± 4				0.283172 ± 3
εHf	14,54	14,40	14,23	14,06	13,60			14,58				14,14

Pre-1960 lavas

	LO08	LO09	LO10§	LO11§	LO12§	LO13	LO14§
Rock type	lava flow	lava flow	lava flow	pebble	pebble	pebble	pebble
Age							
Latitude	S 16° 31' 28.2"	S 16° 31' 29.2"	S 16° 31' 43.7"	S 16° 31' 43.7"	S 16° 31' 43.7"	S 16° 31' 43.7"	S 16° 31' 43.7"
Longitude	E 168° 19' 32.2"	E 168° 19' 39.7"	E 168° 19' 28.9"	E 168° 19' 28.9"	E 168° 19' 28.9"	E 168° 19' 28.9"	E 168° 19' 28.9"
wt %							
SiO_2	50,25	50,56	50,73	52,10	51,86	61,37	54,26
TiO_2	0,77	0,69	0,69	0,82	0,78	0,75	0,87
Al_2O_3	17,11	17,85	17,89	20,10	18,67	16,05	17,45
Fe_2O_3 (t)	11,07	9,74	9,66	9,35	9,49	7,53	9,91
MnO	0,19	0,17	0,17	0,15	0,16	0,14	0,17
MgO	6,16	6,38	6,29	3,24	4,51	2,46	3,93
CaO	11,21	11,64	11,56	10,52	10,24	5,72	8,89
Na_2O	2,46	2,30	2,33	2,92	3,41	3,91	3,33
K_2O	0,64	0,55	0,55	0,66	0,71	1,82	1,00
P_2O_5	0,15	0,12	0,13	0,15	0,16	0,24	0,20
LOI	-0,50	-0,46	-0,43	-0,29	-0,28	-0,32	0,26
Total	100,72	100,57	100,84	100,51	101,04	100,68	99,49
ppm							
Sc	35	34	33	28	32	20	27
V	279	246	257	272	271	149	265
Cr	44	64	59	2	22	4	18
Co	38	33	33	24	30	19	28
Ni	29	36	34	8	16	6	13
Cu	119	120	107	75	97	55	105
Ga	18	16	15	19	19	17	18
Rb	10,8	9,5	9,1	10,8	12,2	32,7	18,0
Sr	304	266	255	280	280	228	263
Y	21,0	19,3	20,0	24,3	25,6	37,3	31,1
Zr	55	49	52	68	76	159	102
Nb	1,29	1,30				3,68	
Cs	0,33	0,27	0,29	0,31	0,21	0,25	0,54
Ba	126	102	103	114	133	251	169
La	4,70	4,57	4,48	5,15	6,05	11,84	8,07
Ce	11,3	10,9	10,6	12,6	14,2	27,8	18,9
Pr	1,75	1,57	1,57	1,87	2,07	3,94	2,79
Nd	8,6	7,7	7,7	9,0	10,1	17,8	13,0
Sm	2,56	2,26	2,29	2,73	2,88	4,70	3,63
Eu	0,90	0,81	0,79	0,94	0,97	1,23	1,10
Gd	3,09	2,74	2,78	3,43	3,56	5,20	4,27
Tb	0,52	0,47	0,49	0,58	0,61	0,88	0,74
Dy	3,52	3,22	3,17	3,86	4,05	5,96	4,80
Ho	0,75	0,69	0,70	0,85	0,89	1,28	1,06
Er	2,21	2,07	2,08	2,50	2,62	3,90	3,17
Yb	2,15	2,00	2,04	2,49	2,56	3,95	3,17
Lu	0,32	0,30	0,30	0,36	0,38	0,60	0,47
Hf	1,56	1,41			2,06	4,19	
Ta	0,084	0,081				0,243	
Pb	2,30	1,88	1,77	1,48	2,68	5,23	3,20
Th	0,54	0,58	0,59	0,61	0,78	1,92	1,08
U	0,24	0,22	0,23	0,27	0,33	0,88	0,49
Isotopes							
$^{87}Sr/^{86}Sr$	0.703961 ± 8 *					0.703937 ± 8	
$^{143}Nd/^{144}Nd$	0.512972 ± 8					0.512994 ± 8	
εNd	6,52					6,94	
$^{206}Pb/^{204}Pb$	18.475 ± 1					18.514 ± 1	
$^{207}Pb/^{204}Pb$	15.543 ± 1					15.542 ± 1	
$^{208}Pb/^{204}Pb$	38.402 ± 3					38.383 ± 2	
$^{176}Hf/^{177}Hf$	0.283181 ± 4					0.283177 ± 3	
εHf	14,46					14,32	

Table 1: continued

	Pre-1960 lavas																Standard				Duplicate	
	LO15	**LO16**	**LO18**	**LO19§**	**LO20**	**LO21§**	**LO22**	**LO23§**	**LO24§**	**LO26§**	**LO27§**	**LO28**	**LO29§**	**LO33§**	**LO34§**	**LO36**	**mean RGM1 (n=36)**	**BCR2 § (n=1)**	**mean JB-2 (n=3)**	**sd**	**LO04§**	**sd**
Rock type	pebble	pebble	pebble	pebble	lava flow	lava flow	lava flow	lava flow	lava flow	lava flow	lava flow	lava flow	lava flow	lava flow	Block	Block						
Age																						
Latitude	S 16° 31' 58.8"	S 16° 31' 58.8"	S 16° 31' 17.3"	S 16° 31' 17.3"	S 16° 32' 04.2"	S 16° 32' 04.3"	S 16° 32' 03.4"	S 16° 32' 01.6"	S 16° 31' 56.8"	S 16° 30' 25.2"	S 16° 30' 31.3"	S 16° 30' 32.5"	S 16° 31' 30.6"	S 16° 31' 17.3"	S 16° 31' 17.3"	S 16° 30' 30.6"						
Longitude	E 168° 20' 05.1"	E 168° 20' 05.1"	E 168° 19' 01.3"	E 168° 19' 01.3"	E 168° 20' 50.2"	E 168° 20' 40.7"	E 168° 20' 27.3"	E 168° 20' 23.9"	E 168° 20' 09.9"	E 168° 20' 26.7"	E 168° 20' 24.0"	E 168° 20' 27.9"	E 168° 20' 26.9"	E 168° 19' 01.3"	E 168° 19' 01.3"	E 168° 20' 23.2"						
wt %																						
SiO_2	49,93	56,13	61,35	52,08	50,64	52,45	52,73	51,23	52,16	52,45	55,31	50,64	52,35	52,43	52,44	54,06	73,43					
TiO_2	0,70	0,79	0,75	0,78	0,58	0,79	0,81	0,81	0,78	0,80	0,66	0,79	0,81	0,80	0,79	0,84	0,27					
Al_2O_3	16,65	17,61	16,06	18,79	16,97	19,75	19,45	17,37	20,36	19,00	16,96	17,30	18,70	18,73	20,09	18,48	13,76					
Fe_2O_3 (t)	10,33	8,85	7,51	9,47	9,31	9,23	9,24	10,39	9,11	9,36	8,67	10,90	9,69	9,48	9,08	9,28	1,90					
MnO	0,18	0,16	0,14	0,16	0,16	0,16	0,16	0,18	0,15	0,16	0,16	0,19	0,17	0,16	0,16	0,16	0,04					
MgO	7,50	3,49	2,49	4,74	7,68	3,70	3,72	5,72	3,43	4,51	5,15	6,04	4,32	4,63	3,55	3,89	0,29					
CaO	11,86	8,27	5,72	10,40	12,08	10,26	10,16	10,99	10,43	10,09	9,02	10,85	10,16	10,09	10,19	9,03	1,19					
Na_2O	2,18	3,32	3,92	2,77	2,05	2,79	2,81	2,49	2,79	2,79	2,85	2,49	2,80	2,81	2,89	3,14	4,10					
K_2O	0,53	1,18	1,82	0,66	0,43	0,72	0,77	0,67	0,64	0,69	1,05	0,66	0,83	0,71	0,66	0,92	4,35					
P_2O_5	0,13	0,20	0,24	0,15	0,11	0,16	0,16	0,15	0,15	0,16	0,16	0,15	0,18	0,16	0,15	0,19	0,05					
loi	-0,44	-0,24	-0,34	-0,28	-0,25	-0,29	-0,34	-0,40	-0,30	-0,10	-0,28	-0,32	-0,12	-0,17	-0,44	-0,37	0,93					
Total	101,16	100,75	100,8	100,63	100,79	100,63	100,61	100,75	100,8	100,49	99,95	100,38	100,02	100,37	101,07	100,92	100,31					
ppm																						
Sc	34	27	18	30	39	29	28	32	28	28	33	35	29	29	29	27	3,8					
V	271	216	146	267	243	255	262	276	265	269	209	287	267	265	280	261	15					
Cr	144	9	5	32	131	8	9	42	2	25	87	41	14	23	0,2	7	2,7					
Co	41	24	19	30	40	26	26	35	24	27	27	35	28	28	25	24	1,2					
Ni	49	11	7	19	51	10	9	26	8	14	32	30	12	16	8	9	3,2					
Cu	119	91	46	100	92	96	105	101	74	81	92	82	104	61	91	84	15					
Ga	16	18	18	18	15	18	18	17	19	18	16	16	17	17	19	18	16					
Rb	9,5	20,9	32,2	8,4	7,6	12,4	12,9	11,5	11,3	11,8	18,3	10,4	13,5	11,3	10,7	16,3		48,0	6,2	0,18	12,3	0,1
Sr	288	254	225	262	240	299	290	299	298	275	244	307	315	271	289	300		359	180	1	353	5
Y	18,6	29,2	36,9	23,8	15,4	24,4	22,9	23,8	23,6	24,3	27,2	21,6	24,0	24,1	23,1	25,8		40,0	24,0	0,2	18,4	0,6
Zr	48	106	157	68	41	67	66	65	65	68	91	55	74	62	62	83		183	47	0,3	52	2,2
Nb	1,17	2,46	3,65		1,01		1,74					1,31				2,02			0,48	0,01		
Cs	0,31	0,53	0,22	0,18	0,24	0,37	0,35	0,36	0,32	0,35	0,53	0,32	0,49	0,12	0,15	0,39		1,33	0,82	0,005	0,40	0,025
Ba	97	177	251	120	75	123	127	134	116	127	161	126	140	122	116	147		700	218	2	135	2
La	4,37	8,44	11,97	5,65	4,10	5,76	5,85	5,25	5,37	5,84	7,18	4,76	6,16	5,82	5,37	7,06		25,5	2,25	0,03	5,18	0,02
Ce	10,8	19,7	27,3	13,2	10,0	13,5	14,0	12,5	12,7	13,7	16,5	11,5	14,9	13,8	13,0	16,5		53,1	6,5	0,05	12,1	0,1
Pr	1,60	2,80	3,92	1,92	1,48	2,00	2,05	1,88	1,88	2,00	2,41	1,75	2,17	1,99	1,89	2,43		7,04	1,14	0,005	1,82	0,01
Nd	8,0	13,0	17,5	9,3	7,2	9,6	9,9	9,1	9,1	9,8	11,2	8,8	10,3	9,6	9,2	11,6		28,8	6,4	0,06	8,7	0,15
Sm	2,36	3,60	4,63	2,68	2,03	2,73	2,80	2,70	2,62	2,74	3,10	2,61	2,99	2,76	2,65	3,21		6,58	2,28	0,01	2,47	0,01
Eu	0,85	1,08	1,22	0,91	0,73	0,95	0,94	0,92	0,91	0,90	0,86	0,93	1,02	0,88	0,92	1,04		1,88	0,85	0,003	0,85	0,004
Gd	2,82	4,16	5,18	3,32	2,39	3,35	3,34	3,29	3,21	3,48	3,70	3,17	3,55	3,54	3,41	3,75		6,89	3,16	0,01	2,81	0,02
Tb	0,47	0,71	0,88	0,58	0,40	0,58	0,57	0,57	0,56	0,58	0,60	0,54	0,63	0,60	0,60	0,63		1,07	0,57	0,003	0,47	0,006
Dy	3,17	4,72	5,91	3,82	2,69	3,78	3,81	3,73	3,66	4,01	4,10	3,57	4,08	3,70	3,78	4,25		6,36	3,99	0,02	2,99	0,05
Ho	0,67	1,02	1,27	0,83	0,58	0,83	0,82	0,82	0,81	0,84	0,92	0,77	0,87	0,88	0,84	0,91		1,33	0,87	0,007	0,67	0,015
Er	2,01	3,10	3,86	2,44	1,73	2,43	2,47	2,36	2,35	2,47	2,70	2,29	2,53	2,51	2,47	2,74		3,75	2,60	0,02	1,94	0,03
Yb	1,91	3,06	3,92	2,42	1,66	2,37	2,40	2,29	2,33	2,48	2,80	2,19	2,43	2,55	2,45	2,69		3,48	2,54	0,02	1,83	0,005
Lu	0,29	0,46	0,60	0,36	0,25	0,36	0,37	0,34	0,35	0,37	0,42	0,33	0,39	0,38	0,38	0,41		0,49	0,38	0,003	0,27	0,004
Hf	1,39	2,85	4,12		1,24		1,88					1,58				2,26			1,47	0,01		
Ta	0,074	0,160	0,241		0,064		0,110					0,084				0,132			0,039	0,0004		
Pb	2,29	3,68	4,49	2,00	1,96	2,32	2,62	2,32	2,12	2,24	3,26	2,13	2,53	1,41	2,21	3,07		9,84	5,18	0,04	2,41	0,09
Th	0,51	1,16	1,92	0,73	0,46	0,68	0,74	0,58	0,61	0,82	1,12	0,54	0,85	0,75	0,66	0,92		5,81	0,26	0,005	0,64	0,004
U	0,21	0,53	0,88	0,30	0,19	0,29	0,32	0,25	0,27	0,32	0,51	0,25	0,35	0,32	0,29	0,39		1,65	0,15	0,002	0,27	0,01
Isotopes																						
$^{87}Sr/^{86}Sr$	0.704001 ± 9 *	0.703938 ± 6	0.703917 ± 10 *		0.703955 ± 8		0.703965 ± 8									0.703977 ± 8			0.703686 ± 6			
$^{143}Nd/^{144}Nd$	0.512965 ± 10	0.512999 ± 6	0.512988 ± 6		0.512984 ± 4		0.512982 ± 10									0.512984 ± 10			0.513089 ± 8			
εNd	6,38	7,04	6,83		6,75		6,71									6,75			8,80			
$^{206}Pb/^{204}Pb$	18.513 ± 1	18.505 ± 0	18.513 ± 1		18.519 ± 1		18.518 ± 1									18.519 ± 1			18.343 ± 1			
$^{207}Pb/^{204}Pb$	15.554 ± 1	15.545 ± 1	15.543 ± 1		15.554 ± 1		15.55 ± 1									15.550 ± 1			15.557 ± 1			
$^{208}Pb/^{204}Pb$	38.439 ± 3	38.395 ± 2	38.381 ± 2		38.435 ± 2		38.425 ± 2									38.423 ± 2			38.265 ± 2			
$^{176}Hf/^{177}Hf$	0.283161 ± 6	0.283179 ± 4	0.283181 ± 9		0.283157 ± 11		0.283175 ± 5									0.283178 ± 5			0.283251 ± 4			
εHf	13,76	14,41	14,47		13,61		14,26									14,34			16,95			

Table 2

Click here to download Table: Table2-AFC.pdf

Table 2: Bulk D values and end member composition (most basic magmas and contaminant) input in the AFC model

		U	Pb	Ba	Yb	Sr	Hf	$^{206}Pb/^{204}Pb$	$^{207}Pb/^{204}Pb$	$^{208}Pb/^{204}Pb$	$^{87}Sr/^{86}Sr$	$^{176}Hf/^{177}Hf$	r
	Bulk D	0.03	0.13	0.11	0.58	0.52	0.11						
Most basic magma	**Pre-1960: LO15**	0.212	2.29	97	1.91	288	1.39	18.513	15.554	38.439	0.704001	0.283161	
	Post-1960: LO03	0.260	2.62	135	1.78	359	1.35	18.512	15.549	38.425	0.704035	0.283174	
Contaminant	**C_a and R_a pre-1960: 1% partial melt**	1.189	2.28	58.2	5.32	176	19.0	18.50	15.48	38.07	0.7033	0.28319	0.2
	C_a and R_a post-1960: 10% partial melt	0.369	1.41	32.7	4.93	159	10.7	17.90	15.48	38.07	0.7033	0.28319	0.3

Figure 1 Color

Click here to download Figure: Fig1-map_vanuatu-color.eps

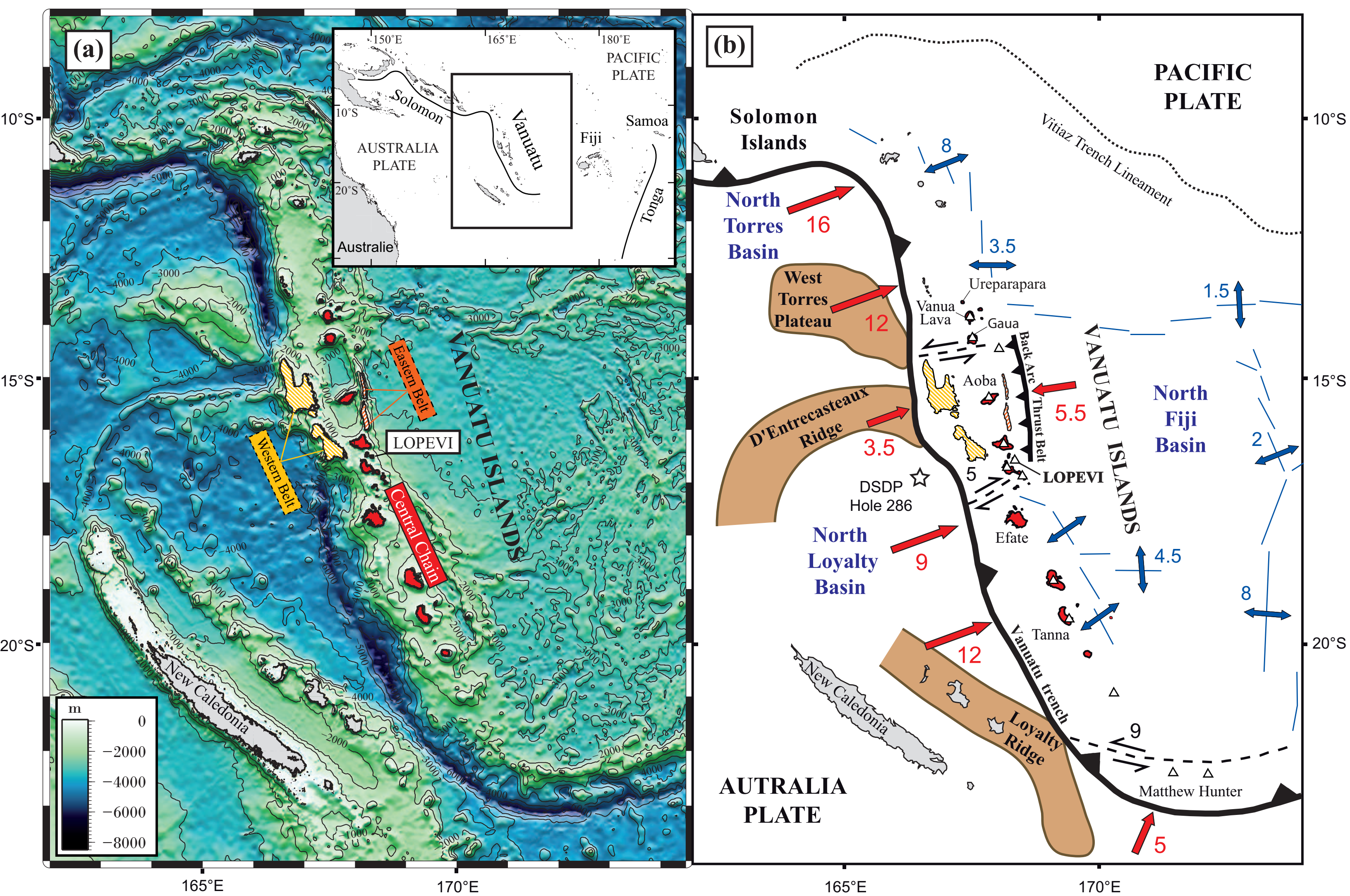

Figure 1

Figure 2 Color

Click here to download Figure: Fig2-map_lopevi_ech-color.eps

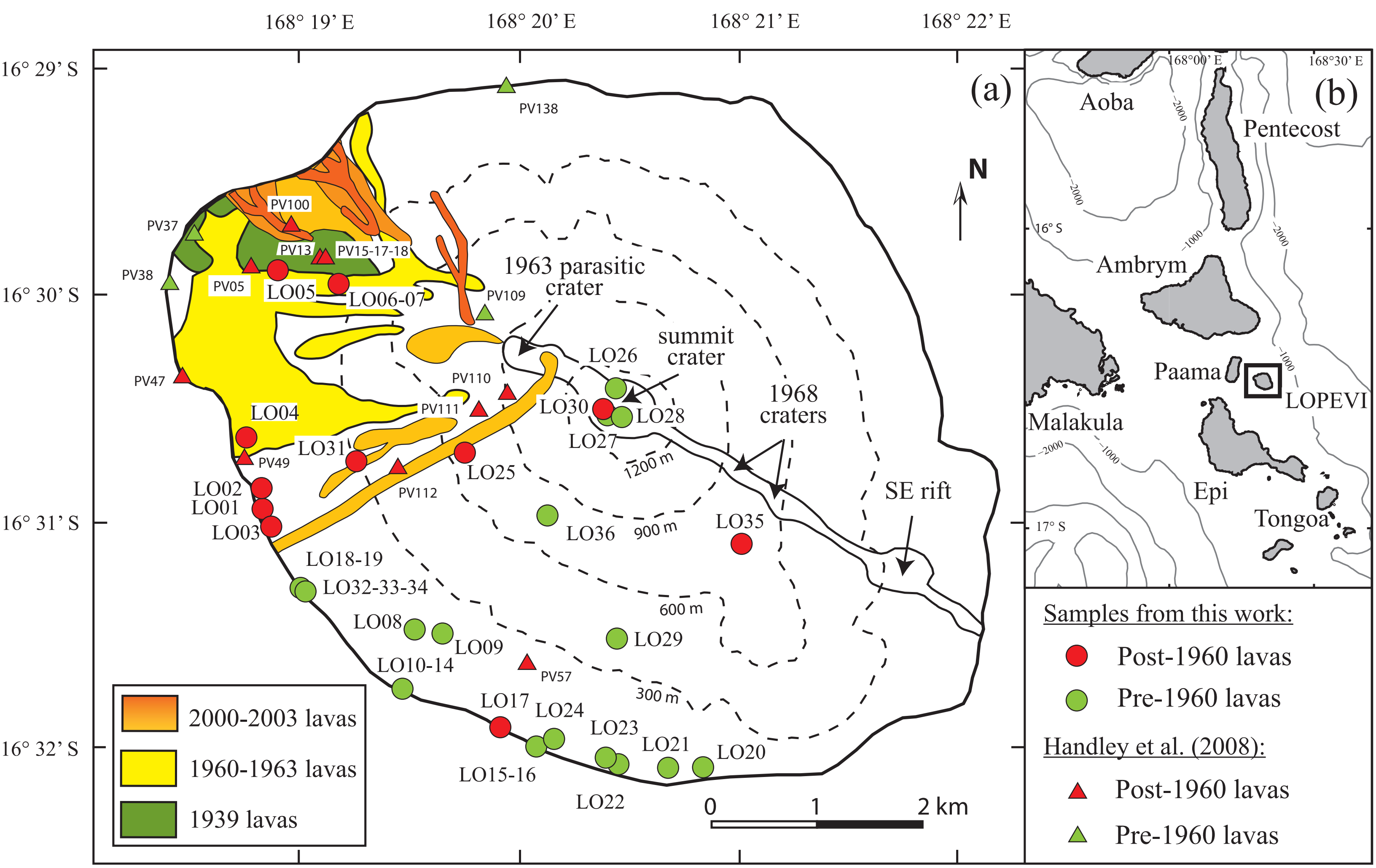

Figure 2

Figure 3 Color

Click here to download Figure: Fig3-K2OvsSiO2-Lop-color.eps

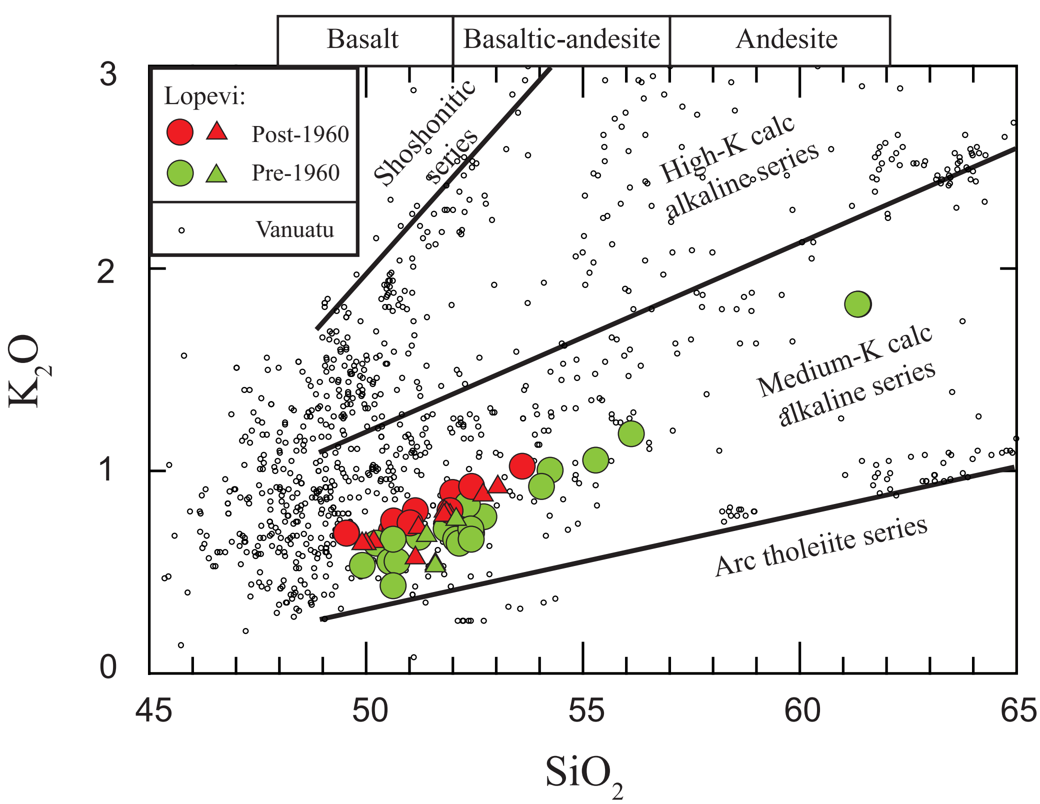

Figure 3

Figure 4 Color
Click here to download Figure: Fig4-Major-Lop-color.eps

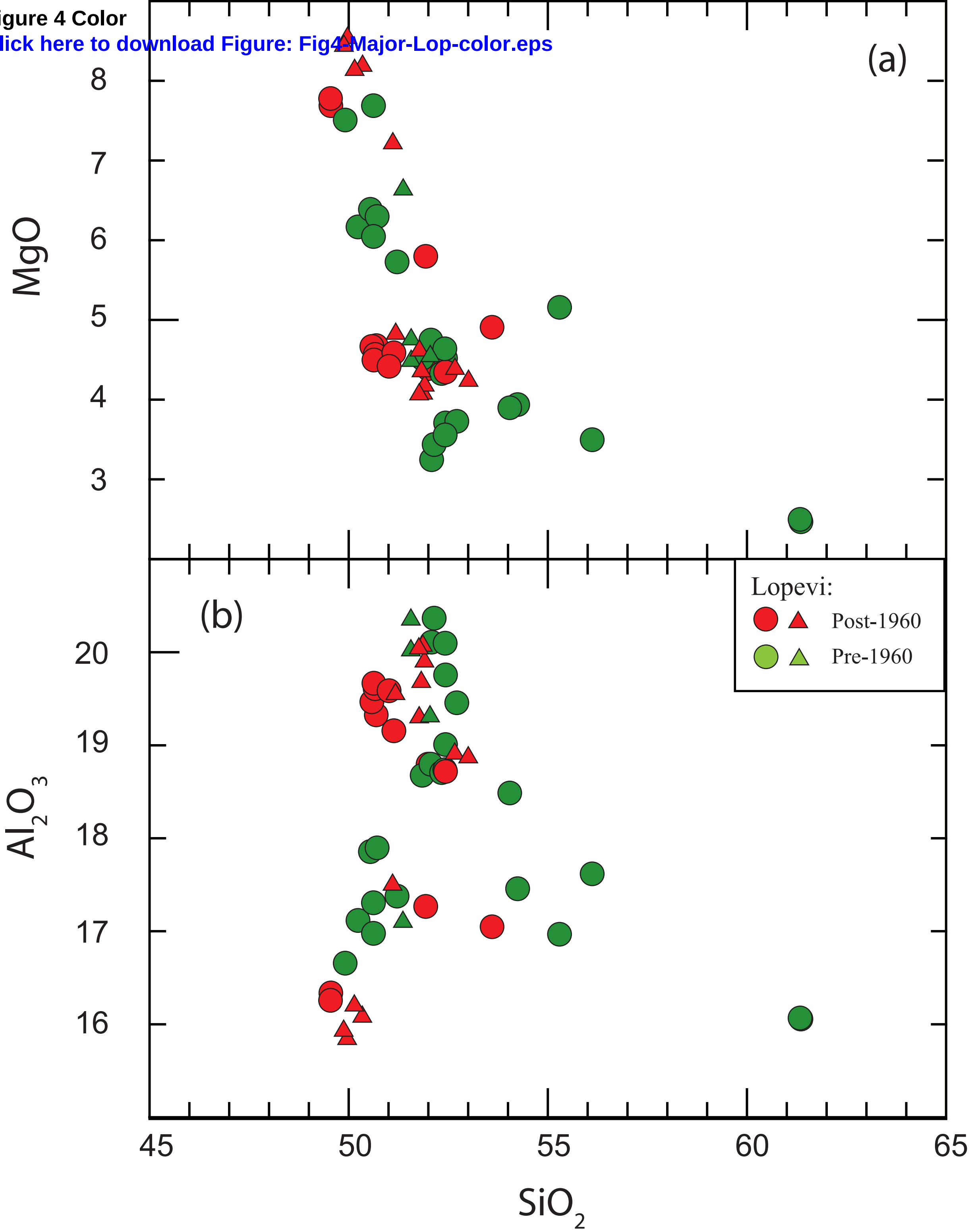

Figure 4

Figure 5 Color
Click here to download Figure: Fig5-Spectre-Lop-color.eps

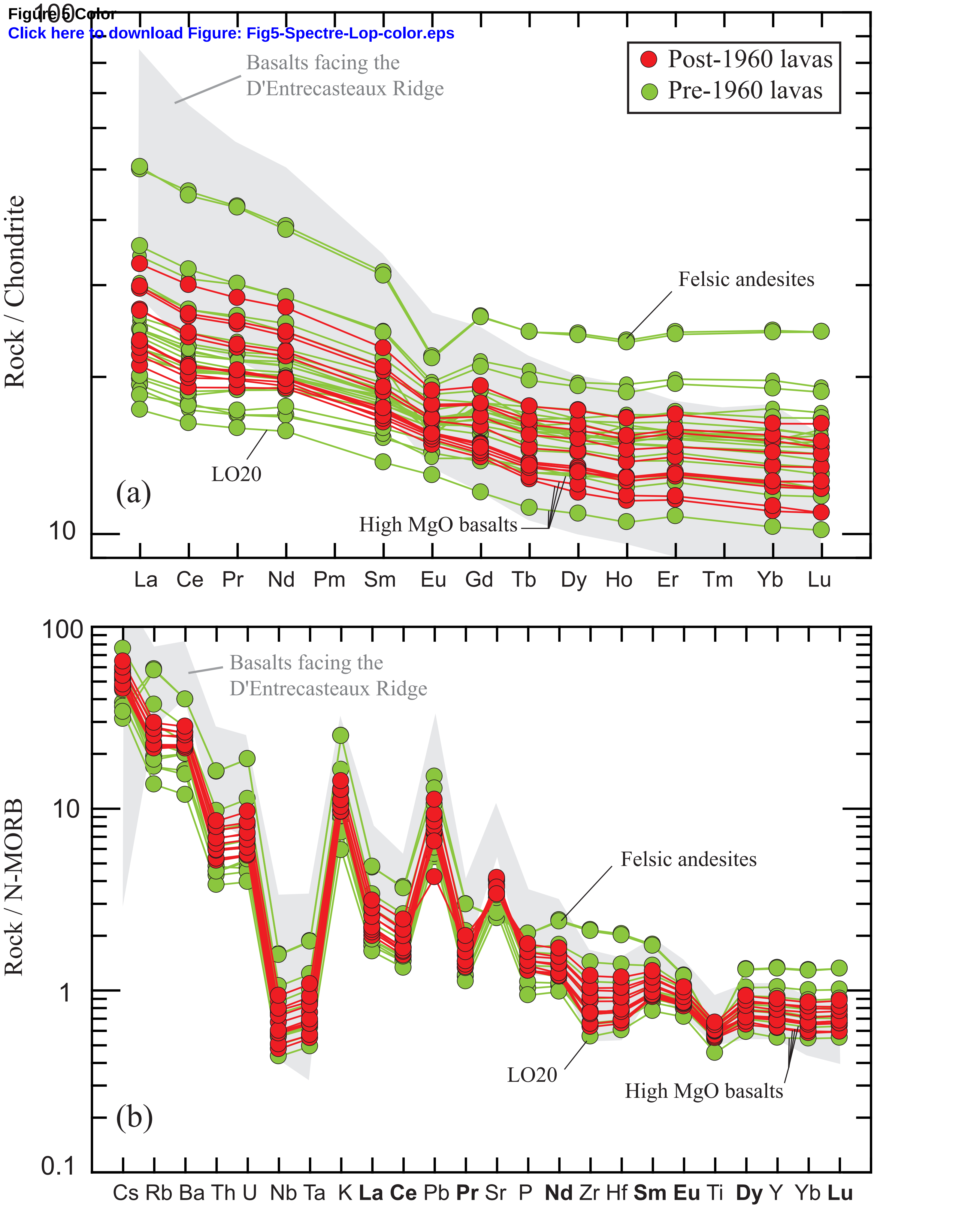

Figure 5

Figure 6 Color
Click here to download Figure: Fig6-ThvsNb-Lop-color.eps

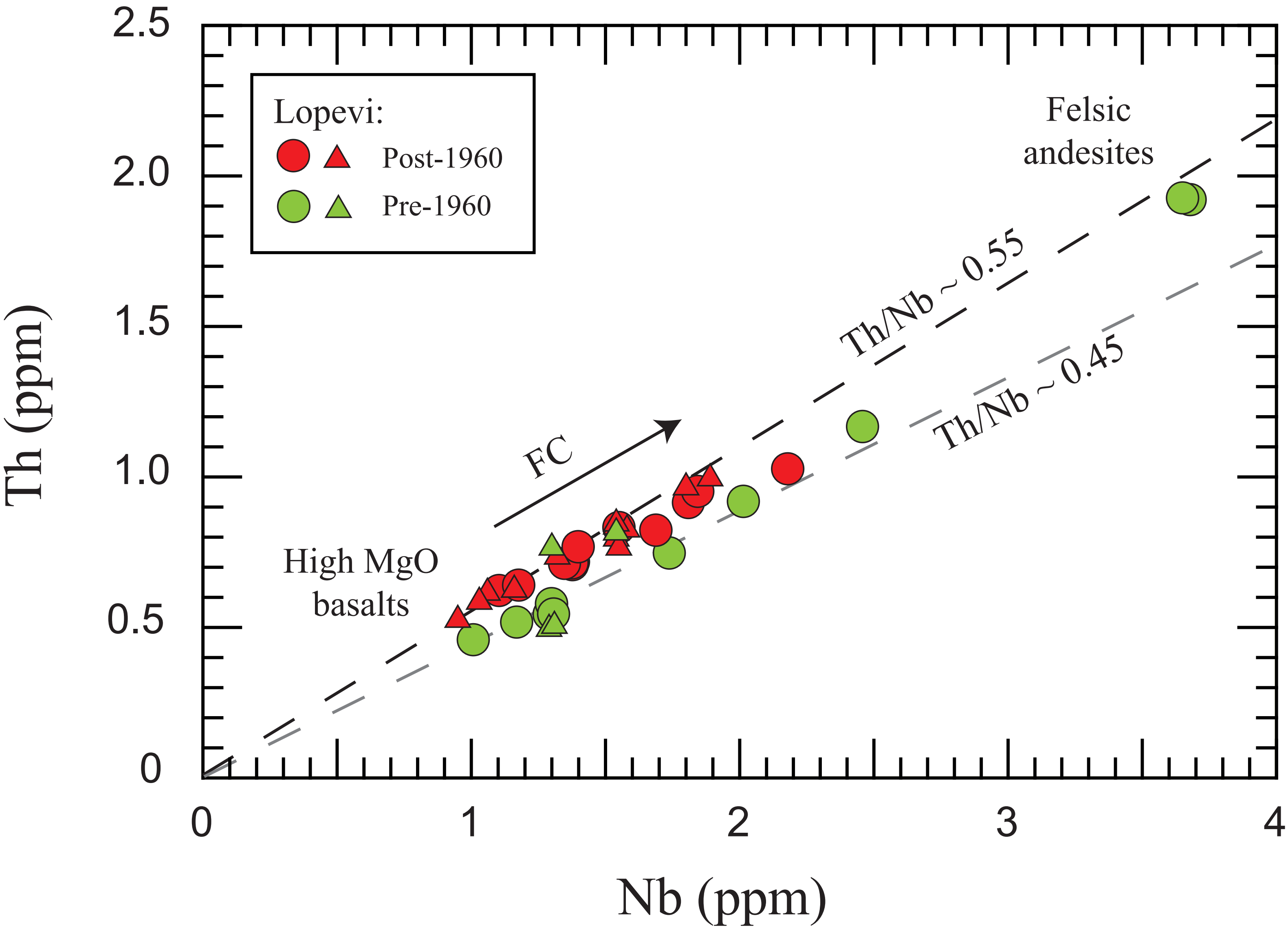

Figure 6

Figure 7 Color

Click here to download Figure: Fig7-Iso-SrNdPbHf-Lop-color.eps

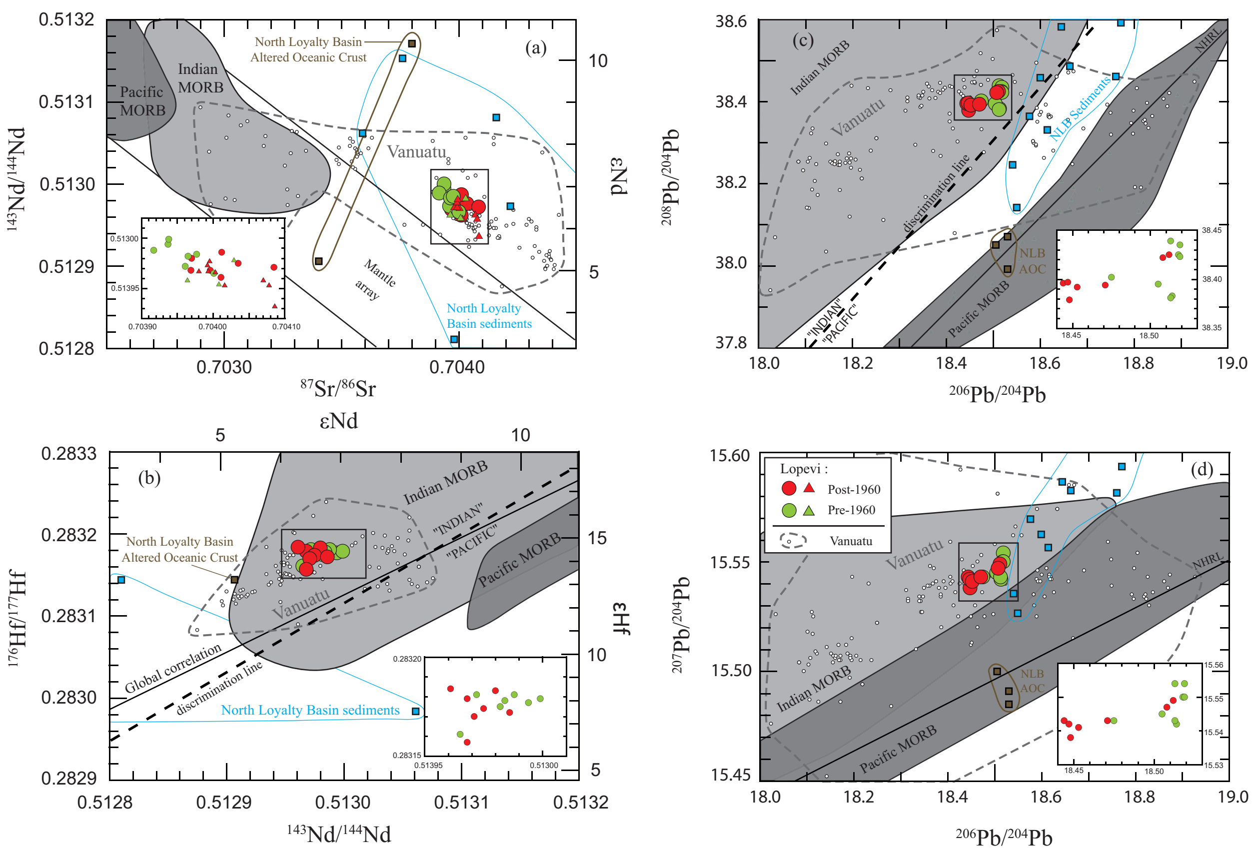

Figure 7

Figure 8 Color
Click here to download Figure: Fig8-AFC_Pb-Sr-NdvsSiO2-color.eps

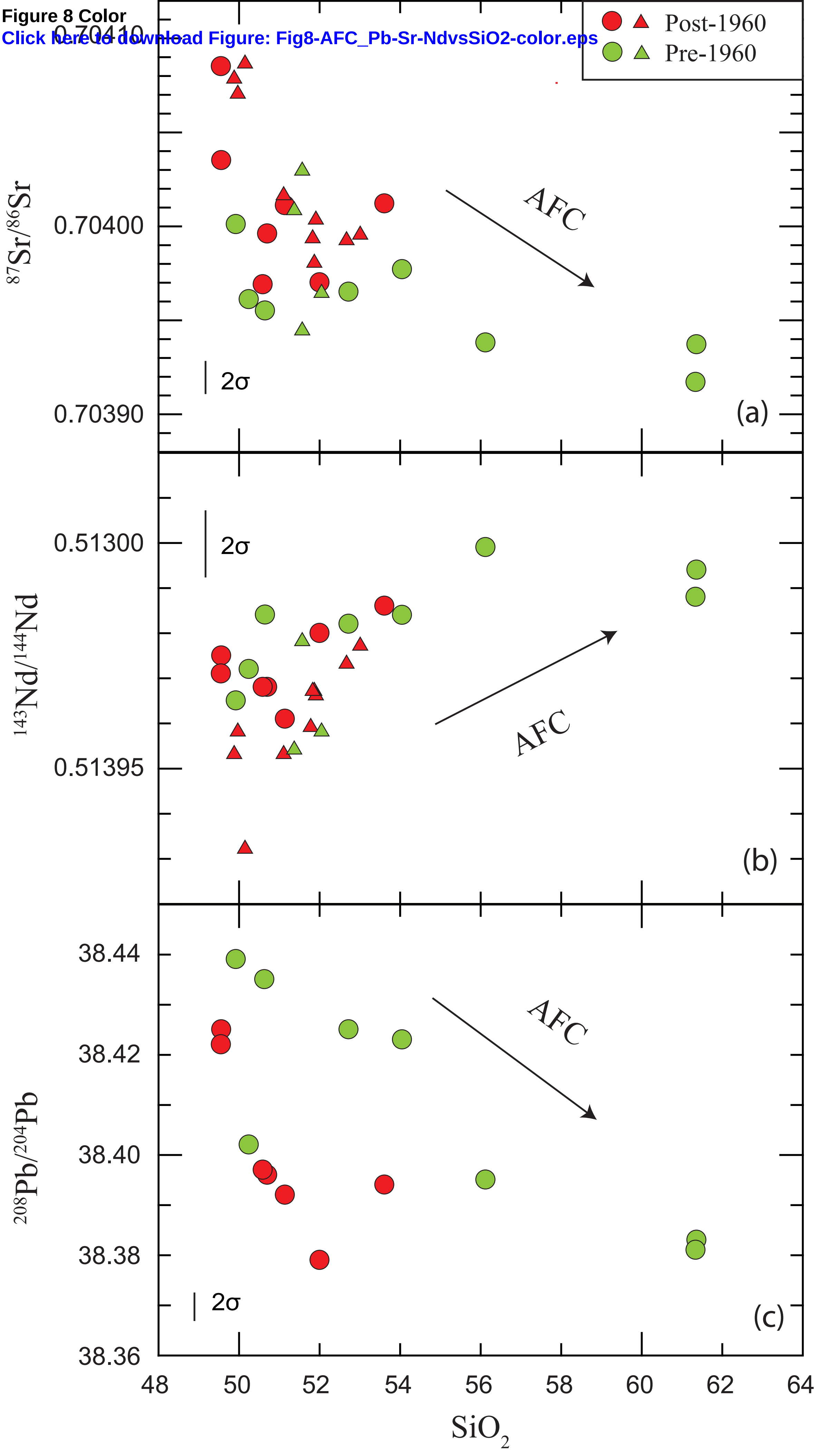

Figure 8

Figure 9 Color

Click here to download Figure: Fig9-AFCmodel-meltOC-color.eps

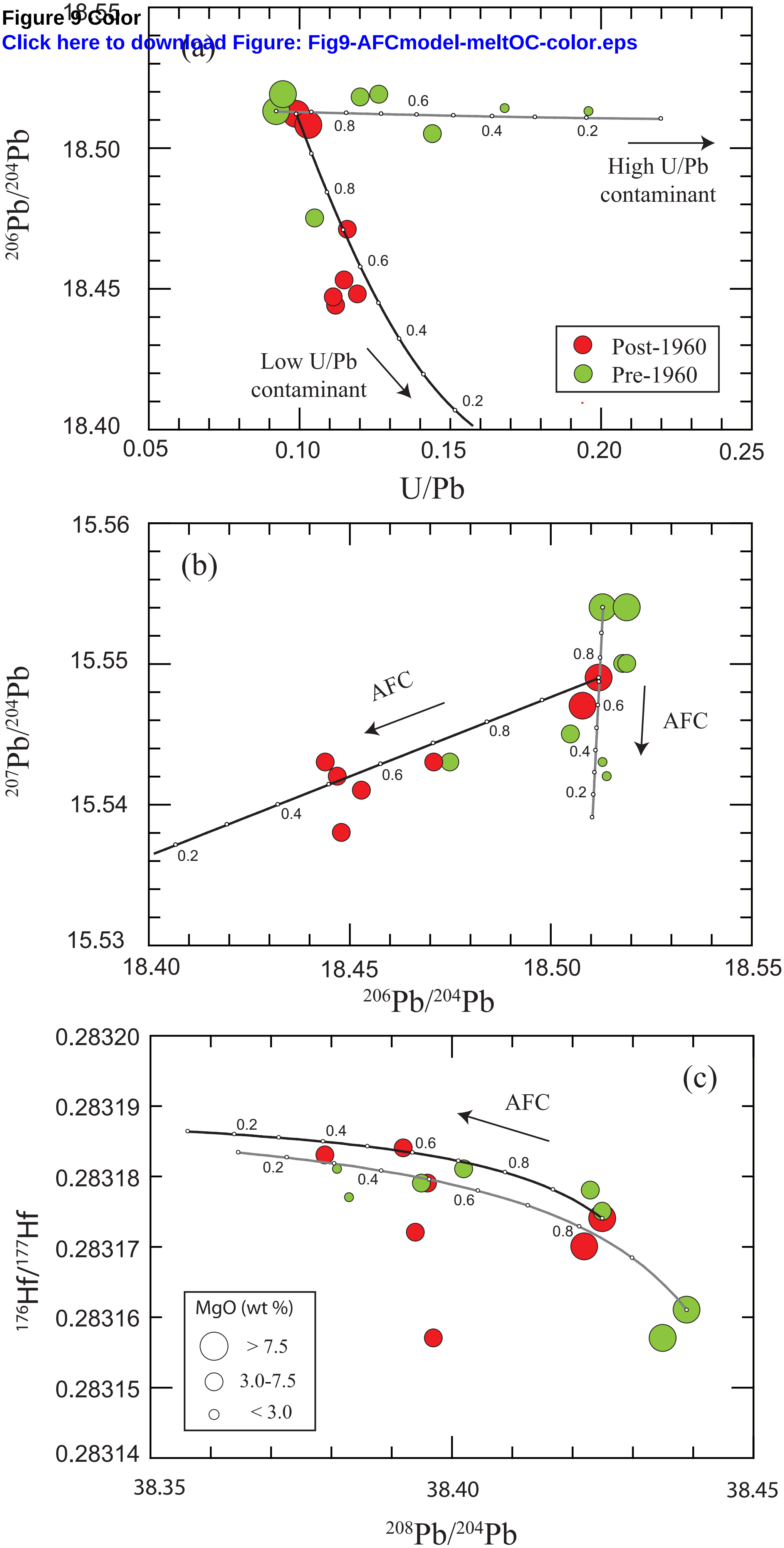

Figure 9

Figure 10 Color

Click here to download Figure: Fig10-TraceRatioDiff-AFCmodel-color.eps

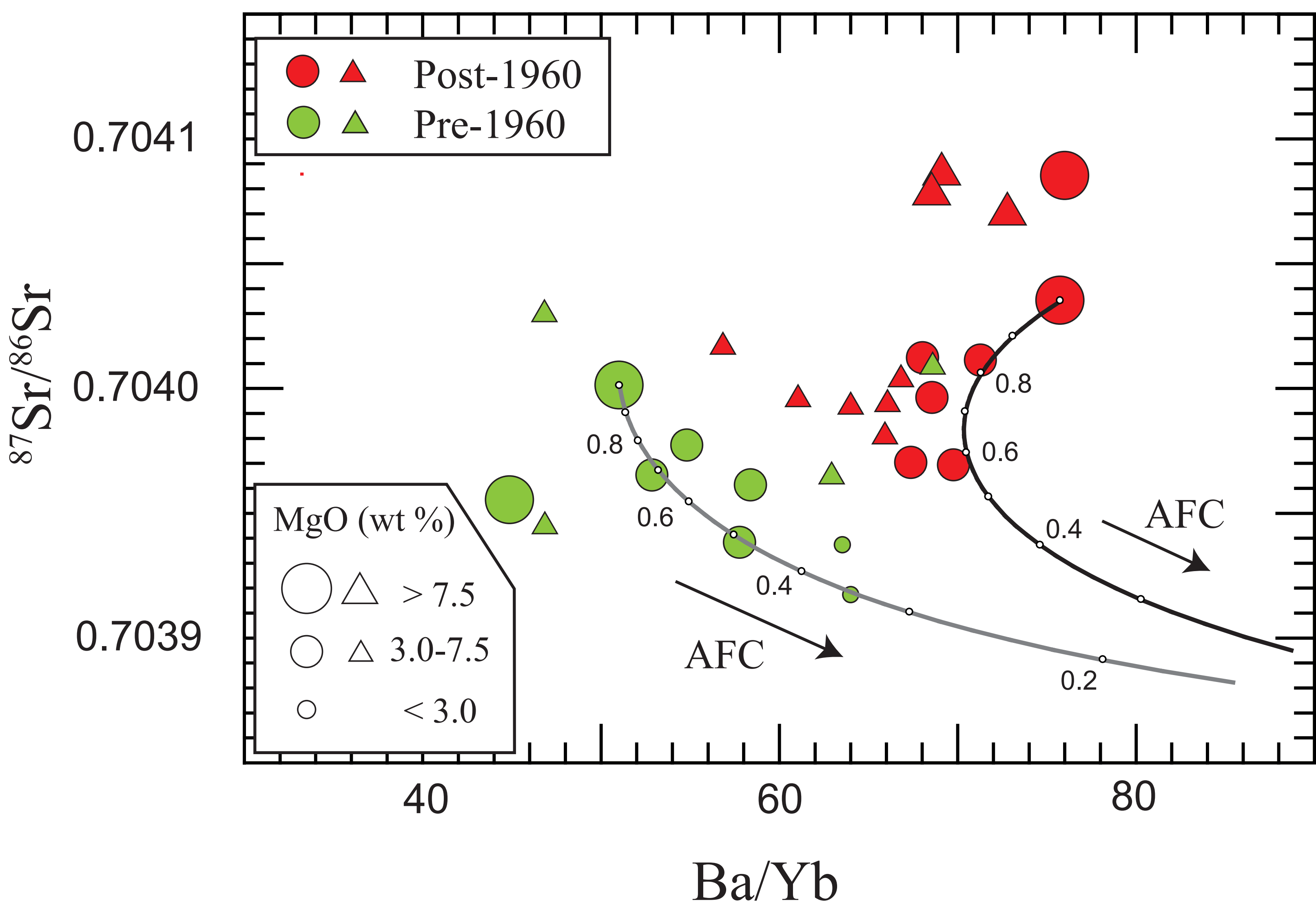

Figure 10

Figure 11 Color

Click here to download Figure: Fig11-Spectre-basalt-color.eps

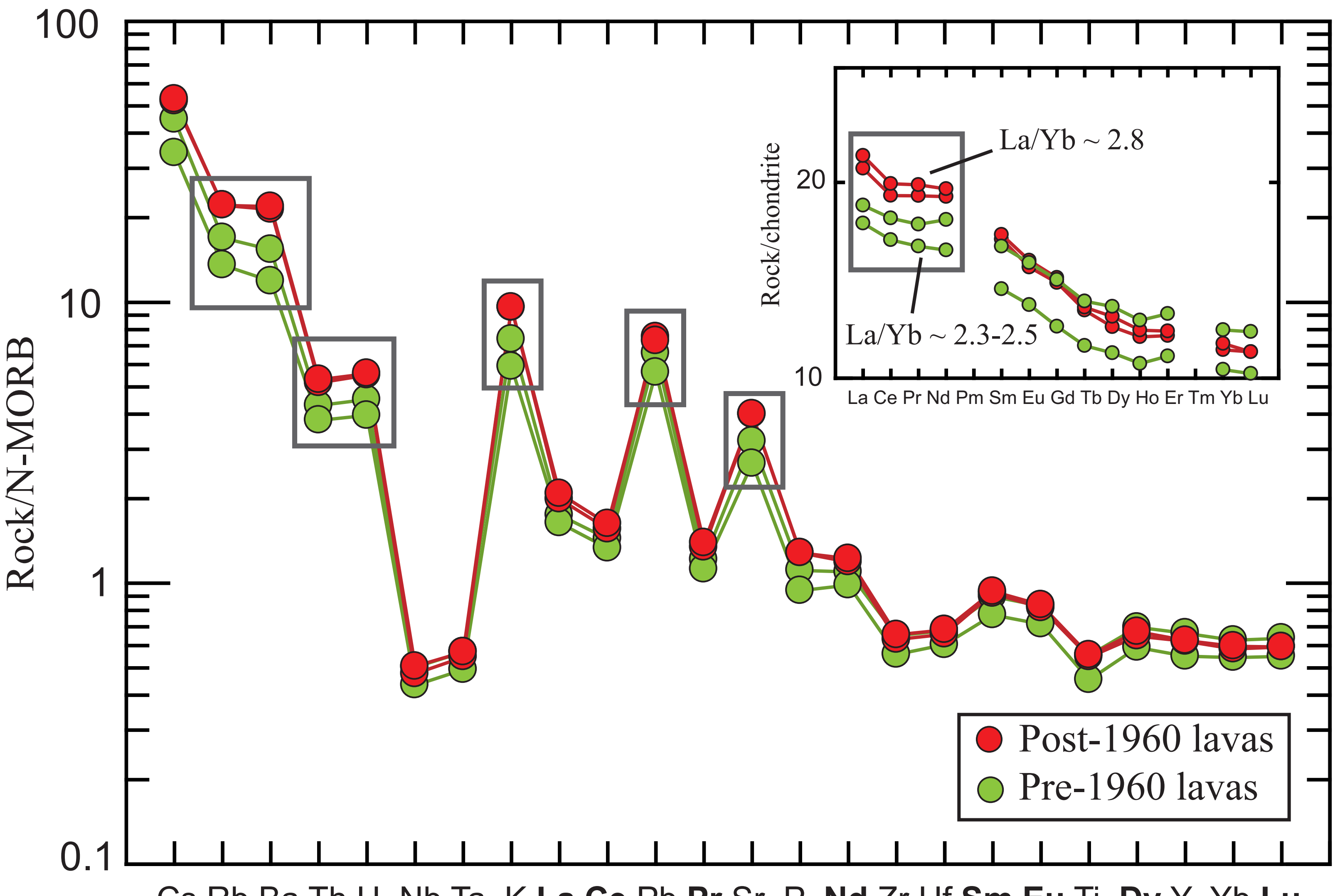

Figure 11